12-10-1997

Beryllium in Lithium-Deficient F and G Stars

Alex Stephens
University of Hawaii

Ann Merchant Boesgaard
University of Hawaii

Jeremy R. King
Clemson University, jking2@clemson.edu

Constantine P. Deliyannis
Yale University

THE ASTROPHYSICAL JOURNAL, 491:339–358, 1997 December 10

BERYLLIUM IN LITHIUM-DEFICIENT F AND G STARS

ALEX STEPHENS[1] AND ANN MERCHANT BOESGAARD[1]
Institute for Astronomy, University of Hawaii at Mānoa, 2680 Woodlawn Drive, Honolulu, HI 96822; alex@galileo.ifa.hawaii.edu, boes@galileo.ifa.hawaii.edu

JEREMY R. KING[1]
Space Telescope Science Institute, 3700 San Martin Drive, Baltimore, MD 21218; jking@unsold.stsci.edu

AND

CONSTANTINE P. DELIYANNIS[1,2,3]
Department of Astronomy, Center for Solar and Space Research, and Center for Theoretical Physics, Yale University, P.O. Box 208101, New Haven, CT 06520-8101; con@athena.astro.yale.edu
Received 1997 February 25; accepted 1997 July 24

ABSTRACT

We present the results of an extensive search, conducted at the Canada-France-Hawaii 3.6-m telescope, for beryllium (Be) in the atmospheres of lithium-deficient F and G dwarfs. We also report revised lithium (Li) estimates for the entire sample using previously published equivalent widths and updated, consistently calculated stellar parameters. Abundances derived from an LTE analysis of the Li and Be line-forming regions confirm the suspicion that F stars which deplete Li by factors of 10–200 may also be beryllium deficient. Photospheric Be concentrations range from near meteoritic levels in G dwarfs to factors of 10–100 below this assumed initial abundance in hotter stars. Moreover, significant Be deficiencies appear in stars that populate a 600 K wide effective temperature window centered on 6500 K. This Be abundance gap is reminiscent of the Li gap observed in open clusters. Also, the discovery of 12 probable "110 Herculis" stars, objects that exhibit a depleted, *but detected*, surface concentration of both Li and Be, provides a powerful means of differentiating between the possible physical processes responsible for observed light element abundance patterns. Indeed, the Be data presented here, in conjunction with the newly calculated Li abundances, lead to the following conclusions regarding the hypothesized, light element depletion scenarios: Mass loss cannot account for stars with severely depleted (but detected) Li and moderate Be deficiencies. The predicted timescales for surface depletion due to microscopic diffusion are too long for significant Li and Be deficiencies to develop in cool ($T_{\rm eff} \leq 6200$) stars; nevertheless, underabundances are observed in these stars. Diffusion theory also predicts Li and Be depletion rates to be comparable, but it is evident that Li and Be depletion proceed at different speeds. Models of mixing induced by internal gravity waves cannot explain mild Be deficiencies in cool dwarfs. A key meridional circulation prediction regarding the efficiency and severity of Li and Be dilution is shown to be fallible. However, rotationally induced mixing, a turbulent blending of material beneath the surface convection zone due to the onset of instabilities from superficial angular momentum loss, predicts both the observed light element depletion morphology as well as the existence of 110 Her analogs. These "Yale" mixing models provide, therefore, the most plausible explanation, of those presented, for the observed Li and Be abundances.

Subject headings: stars: abundances — stars: interiors — turbulence

1. INTRODUCTION

The light elements lithium (Li), beryllium (Be), and boron (B), delicate atoms susceptible to destructive fusion reactions within stellar interiors, are useful probes of the regions beneath the surface convection zone in cool, main-sequence stars. The degree to which Li, Be, and B are depleted from a stellar atmosphere serves as a subtle tracer of internal stellar kinematics. Physical processes may either remove the fragile trio from contact with the surface convection zone or destroy them outright. These light elements, like a drop of dye highlighting currents in a glass of water, provide information regarding the redistribution of material and mixing patterns within a star. Spectroscopic studies of Li, Be, and B therefore expose the otherwise hidden stellar interior; thus, any future treatment of the structure or evolution of stars should incorporate the physical processes illuminated by observations of the light elements.

Standard stellar evolution models, which ignore complications such as magnetic fields, mass loss, rotation, etc., suggest lithium survives only in the outermost layers (2% by mass) of a typical F dwarf (Pinsonneault, Kawaler, & Demarque 1990). At greater depths, thermal protons easily destroy this low coulomb potential nuclide. However, the bottom of the surface convection zone in a main-sequence F star is far too shallow (less than 0.5% by mass for late F stars and much smaller for early F stars) to drag Li beneath this "destruction depth." Superficial Li abundances in an ordinary F dwarf should therefore resemble its "Li of formation," but some F stars exhibit a significant Li deficiency with respect to an assumed initial abundance. In particular, a Li abundance gap, or dip, which spans a small effective temperature window ($\Delta T \sim 600$ K) centered on $\sim$6600 K, appears to form and strengthen during the main-sequence lifetime of galactic cluster and field stars (see Michaud &

[1] Visiting Astronomer, Canada-France-Hawaii Telescope, which is operated by the National Research Council of Canada, the Centre National de la Recherche Scientifique of France, and the University of Hawaii.
[2] Hubble Fellow.
[3] Beatrice Watson Parrent Fellow, Institute for Astronomy, University of Hawaii at Mānoa.

Charbonneau 1991 for a review). These pathological F dwarfs therefore call into question the completeness of the physics incorporated into the so-called standard model.

Subsequent to the discovery of the Li (or "Boesgaard") gap and the realization that the standard model may lack some fundamental physical principles (Boesgaard & Tripicco 1986a), several possible explanations for the dip appeared in the literature. These explanations include diffusion (Michaud 1986; Richer & Michaud 1993), internal gravity waves (Garcia-Lopez & Spruit 1991; Montalbán 1994), mass loss (Schramm, Steigman, & Dearborn 1990), meridional circulation (Charbonneau & Michaud 1988), rotationally induced mixing due to angular momentum loss (Pinsonneault et al. 1989, 1990; Charbonnel, Vauclair, & Zahn 1992; Charbonnel et al. 1994), and turbulent mixing (Vauclair 1988). Some of these hypotheses attempt to explain and model only the Li abundance gap, but it is reasonable to assume other, structurally similar, atoms will be affected by the proposed depletion mechanisms.

Beryllium, like Li, is a fragile atom easily destroyed by nuclear reactions in the interiors of F and G stars. Whereas Li astration occurs at temperatures near 2.5×10^6 K, similar (p, α) reactions annihilate Be in slightly warmer (deeper) environments ($T \sim 3.5 \times 10^6$ K). The fragility of Be makes it a useful probe of the dynamics linking the surface convection zone and the depth of nuclear destruction because the physical processes acting to deplete Li in cool stars may also affect superficial Be concentrations. Using ground-based telescopes to detect stellar Be is, however, a challenge because the best observable Be feature, the Be II resonance doublet ($\lambda\lambda = 3130.420$ Å and 3131.064 Å), lies near the atmospheric ultraviolet (UV) cutoff. Furthermore, in cool stars with near-solar metallicities, the Be wavelength region is particularly crowded by metallic and molecular absorption lines. Thus, the extraction of reliable Be equivalent widths, especially in the blurred spectra of rapidly rotating stars, is difficult.

To date, a systematic search for Be in Li-deficient stars has been restricted to open clusters such as the Hyades (Boesgaard, Heacox, & Conti 1977; Boesgaard & Budge 1989; Garcia López, Rebolo, & Pérez de Taoro 1995) and a few field stars (Boesgaard 1976; Boesgaard & Lavery 1986), and modest evidence for Be depletion exists in these studies. In an attempt to expand upon these previous works and to explore the possibility that Be may be exhausted in Li-poor stars, we present observations of Be in F and G dwarf field stars. Data reductions and the methods used to extract Be equivalent widths are described in §§ 2 and 3, respectively. The calculation of stellar parameters and abundances are outlined in § 4. Finally, abundance correlations and the ramifications for light element depletion scenarios are presented in § 5.

2. OBSERVATIONS AND DATA REDUCTION

The data presented in this study represent a subset of a larger survey for Be in cool stars that also includes the work of Boesgaard & King (1993, hereafter BK93). Details of the data acquisition and processing procedures appear in BK93; therefore, only the salient features of the reductions will be reiterated below.

Observations of the Be II resonance doublet using the Canada-France-Hawaii 3.6 meter telescope (CFHT) and UV optimized coudé spectrograph were obtained on the following UT dates: 1989 July 12–13 (run 1), 1990 October 2–3 (run 2), 1991 April 4–5 (run 3), 1991 July 2–4 (run 4), and 1992 July 17–19 (run 5). Standard IRAF tasks were used to pre-process (bias subtract, flat field, etc.) and aperture-extract the two-dimensional images. Wavelength rectification of the extracted, one-dimensional spectra required fitting a low-order polynomial to known reference features from a Th-Ar lamp. The dispersion solution consistently resulted in a linear scale of 0.067 Å pixel^{-1} for each of the five observing runs. Lastly, the low spatial frequency shape of each spectrum was fit with a polynomial using three high points ($\lambda\lambda = 3124.5$, 3128, and 3129.5 Å) as "true" continuum markers. Stars with near-solar metallicities were then shifted in relative intensity so that the continuum markers coincided with the position of similar continuum windows in the Kurucz et al. (1984) solar atlas. This "boot-strapping" technique provided a self-consistent means of normalizing the line-blanketed spectra. Sample spectra representative of those obtained during runs 1–5 appear in Figure 1.

We also present high-resolution observations of Be in Li-deficient F and G dwarfs obtained on UT 1995 October 12–15 at the CFHT (run 6). The UV optimized f/4 coudé mirror train and GECKO echelle spectrograph coupled with the UV sensitive Orbit 1 CCD (80% efficient at 3100 Å) allowed us to acquire high signal-to-noise ($\sim$70 pixel^{-1}) spectra at a resolution of $\lambda/\Delta\lambda \sim 120{,}000$. Examples of the spectra acquired on the 1995 October run are presented in Figure 2. For consistency, reduction of the GECKO data mimicked the procedures described in BK93 and above. Preprocessing steps included individually trimming, bias subtracting, cosmic-ray cleaning, and flat-fielding the data using general IRAF tasks. Although the GECKO's free spectral range is small in the UV, the angular dispersion of the cross-dispersing grism was large enough to prevent overlap of adjacent orders. Fitting, and subsequently subtracting, a low-order Legendre polynomial to the interorder

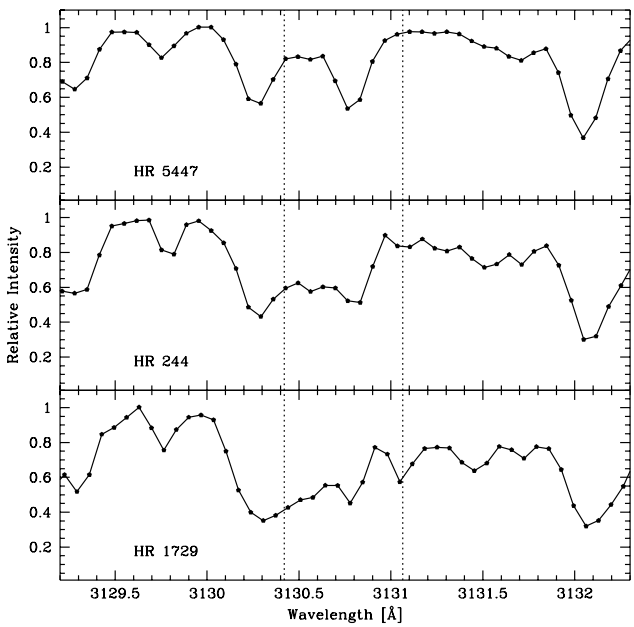

FIG. 1.—Sample spectra of the wavelength region surrounding the Be II resonance doublet. Dotted vertical lines denote the position of the 3130.420 and 3131.064 Å Be II features. These moderate resolution ($\lambda/\Delta\lambda \approx 20{,}000$) spectra, characteristic of runs 1–5, reveal (*bottom-to-top*) progressively smaller Be II absorption lines.

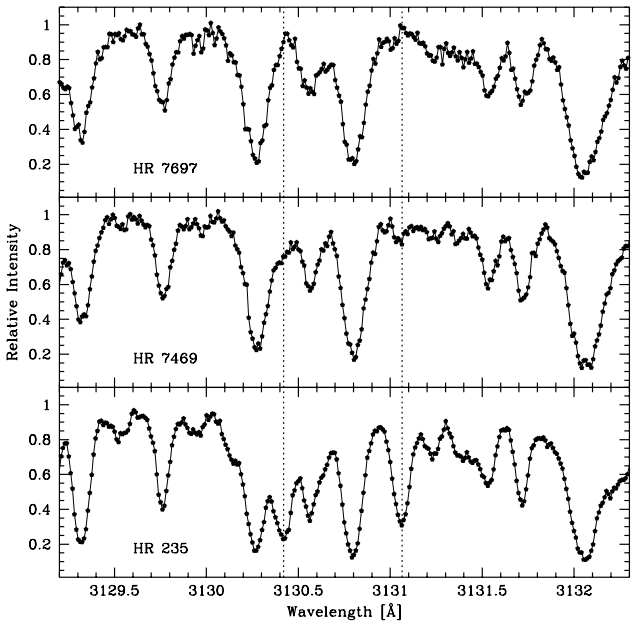

FIG. 2.—Similar to Fig. 1 except the spectra are examples of those obtained with the CFHT and GECKO echelle spectrograph. The spectral resolution ($\lambda/\Delta\lambda \approx 120{,}000$) allows us to resolve the Be 3131.064 Å feature in extremely beryllium-deficient stars such as HR 7469.

region (perpendicular to the dispersion) allowed us to remove any background or scattered light plateau present in the data. Following these preprocessing and cleaning steps, the two–dimensional images were aperture extracted, and the resulting spectrum was placed on a linear wavelength scale using 12 lines from a Th-Ar lamp and a fourth-order Chebyshev polynomial (rms residuals $\sim$0.3 mÅ). The observed dispersion was 0.01 Å pixel^{-1} and the FWHM of a typical calibration line was $\sim$2.7 pixels, resulting in an operating spectral resolution of $\sim$0.027 Å. The final reduction steps included co-adding multiple exposures of a single object, when necessary, and the normalization of all spectra using the boot-strapping method outlined in the preceding paragraph.

Table 1 lists the program stars, the run during which the spectra were acquired, and the calculated per pixel signal–to–noise (S/N) in the Be region.

3. LITHIUM AND BERYLLIUM EQUIVALENT WIDTHS

3.1. *Beryllium*

Gauging the amount of beryllium present in stellar atmospheres typically involves one of two procedures: either matching line strengths to a theoretical curve of growth (CoG) or comparing synthetic spectra, with a "dialed-in" Be abundance, to an observed stellar spectrum. This study relies predominantly on a hybrid curve-of-growth technique to estimate photospheric Be; thus, measured line strengths, or equivalent widths (EQWs), are central to the analysis. Unfortunately, the thicket of metallic and molecular lines that riddle the Be wavelength region pollute the blue feature of the resonance doublet, rendering it virtually unmeasurable. Only the 3131.064 Å line, which is a relatively pristine feature, could have its EQW routinely determined. Line strengths were typically measured using the standard spectral line analysis packages within IRAF. However, spectra with a poorly defined or severely blended Be line required employing additional processing steps to reveal the obscured absorption feature. We relied on two techniques, differential spectroscopy and profile reconstruction, to unveil the red Be II line. Once exposed, IRAF "splot" tasks were used to assess the line strength of the revealed feature.

3.1.1. *IRAF splot Tasks*

The IRAF "splot" package allows one to calculate a line strength using a Gaussian function with a width specified interactively by the user. The computed area beneath the Gaussian "fit" defines a feature's equivalent width. This fitting technique, the same described in BK93, is depicted in Figure 3. Although we rely heavily on this method to estimate EQWs, the robustness of this technique begins to break down, or at least becomes increasingly subjective, as line strengths decrease. We therefore restrict the use of this technique to features with well-defined cores. A somewhat different, but less accurate, means of estimating an EQW in IRAF is the straight pixel summation task. By marking a pair of continuum points, IRAF will compute the area beneath the continuum bounded by the spectral line. This method of estimating line strength turns out to be preferable to the Gaussian profile fit when the Be feature is weak, irregular, or poorly defined.

3.1.2. *Differential Spectroscopy*

Differential spectroscopy provides a means of revealing absorption lines in stars that suffer significant rotational line broadening. Boesgaard & Budge (1989) describe the procedure in detail, but a summary of the technique is warranted. Using a high signal-to-noise (S/N) spectrum of a Be-poor, narrow-lined star as a "template," we subtract this template from an "object" spectrum that has a weak, but detectable, Be absorption feature. If the object and template star are well matched—both have similar stellar parameters—then the two stars will have nearly identical spectra, save, of course, for the strength of the Be line. Template subtraction will therefore reveal the object's hitherto unmeasurable Be resonance doublet.

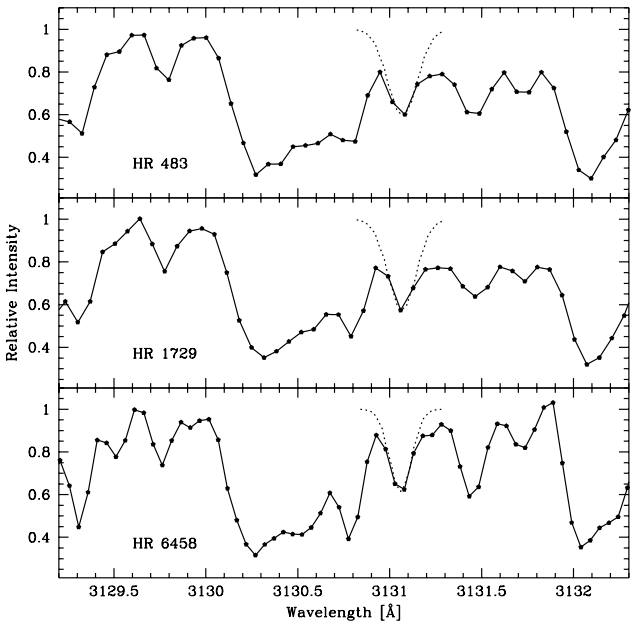

FIG. 3.—Examples of Gaussian fits applied the to 3131.064 Å Be II resonance line.

TABLE 1

OBSERVATIONS AND EQUIVALENT WIDTHS

HD Number	HR Number	Observation Code	S/N	Be (mÅ)	Method[a]	σ(Be)	Li + Fe (mÅ)	Li References
4614.....	219	6	47	83	I	15	20	1, 3
4813.....	235	6	72	88	I	8	66	1, 10
5015.....	244	2	49	31	R	5	<2	1
10307.....	483	2	57	82	I	10	<21	7
13555.....	646	6	81	78	I	10	70	1, 2
19994.....	962	2	92	83	R	10	21	8
30649.....	...	2	70	72	I	5	18	1, 3
34411.....	1729	2	67	84	I	11	<17	7
61421.....	2943	K	210	<5	I	...	<2	1
64096.....	3064	3	39	94	I	10	25	3, 8, 10
65583.....	...	3	41	64	I	8	<9	3
90508.....	4098	3	45	79	I	15	n/a	...
101606.....	4501	3	63	<10	I	...	<2	4
106516.....	4657	3	47	<10	I	...	<5	1, 3, 4
110897.....	4845	3	46	85	I	15	20	1
113022.....	4926	3	35	<20	I	...	<7	4
114762.....	...	3	37	80	I	20	21	1, 3, 5
117176.....	5072	4	34	73	R	10	33	7
119288.....	5156	3	48	<15	I	...	<2	4
126141.....	5387	4	44	53	R	15	<5	4
128093.....	5445	4	50	<18	R	...	<3	2, 4
128167.....	5447	1	73	<5	I	...	<4	1, 9
128429.....	5455	4	23	<25	R	...	<5	2, 4
130817.....	5529	4	49	<25	R	...	<2	2, 4
142373.....	5914	2	13	95	I	10	54	1, 3, 9
145976.....	6052	4	44	35	R, D	15	32	4
146233.....	6060	4	29	85	R	20	15	7
148816.....	...	3	47	80	I	10	18	3, 6
150177.....	6189	4	37	72	I	7	38	4
154417.....	6349	4	31	78	R	15	79	3
156897.....	6445	5	43	<30	R	...	<5	4
157089.....	...	3	41	88	I	7	23	3, 6
157214.....	6458	1	92	60	I	8	<4	6
157373.....	6467	4	44	<15	I	...	<4	2, 4
159332.....	6541	3	47	35	R, D	8	<6	1, 2, 4
160693.....	...	4	33	49	I	10	<6	3, 5
161023.....	6600	4	27	<10	I	...	<3	4
165908.....	6775	1	38	74	I	5	38	1, 6
166285.....	6797	3	38	18	R	6	<6	4
168151.....	6850	5	23	32	R	9	<3	1, 4
173667.....	7061	5; 6	55; 118	38; 50	D; R	5; 15	6	2, 9, 10
182101.....	7354	6	73	54	I	6	7	2, 4
184499.....	...	4	46	70	I	15	9	5
185395.....	7469	6	53	12	I	4	<1	9
191195.....	7697	6	45	<5	I	...	5	2
192455.....	7727	1	11	<15	I	...	<7	2, 4
192985.....	7756	1	71	<5	I	...	<4	4
195633.....	...	4	28	75	I	10	40	5
198390.....	7973	4	47	70	I	10	20	4
200790.....	8077	6	63	22	I	5	<4	2
204121.....	8205	4	49	37	R, D	7	19	2, 4
207978.....	8354	2	90	<12	I	...	<6	2, 3, 4
208906.....	...	2	50	67	I	9	44	1, 3, 5
211976.....	8514	4	57	80	I	10	23	4
218470.....	8805	6	38	<20	I	...	<5	1, 2, 4
220117.....	8885	4; 6	60; 72	60; 60	D; R	10; 15	5	4
222368.....	8969	1	68	81	I	10	23	1, 2, 6, 9
224930.....	9088	1	58	68	I	6	<5	3, 6
225239.....	9107	2	46	95	I	6	32	6

[a] EQW extraction/measurement techniques: (I) IRAF Gaussian fit or pixel summation techniques; (R) profile reconstruction + IRAF splot tasks; (D) differential spectroscopy + IRAF splot tasks.

REFERENCES.—(1) Lambert et al. 1991; (2) Balachandran 1990; (3) Hobbs & Duncan 1987; (4) Boesgaard & Tripicco 1986a, 1986b; (5) Rebolo et al. 1988; (6) Spite & Spite 1982; (7) Duncan 1981; (8) Pallavicini et al. 1987; (9) Boesgaard & Lavery 1986; (10) Boesgaard et al. 1988.

The mechanics of differential spectroscopy is straightforward. With the assistance of cross-correlation techniques, we align the template and object in wavelength space. If necessary, the template is convolved with a Gaussian function in order to match its line width to that of the Doppler-broadened object spectrum. We also may apply a straight vertical shift or a low-order polynomial to the template in order to bring its relative intensity in line with the object continuum. The shifted, broadened template is subtracted from the object, and the residual Be line is measured using

the techniques described in § 3.1.1. A high S/N (~210) spectrum of Procyon (HR 2493—Be ≪ 5 mÅ) acquired at the W. M. Keck 10 m telescope (Boesgaard et al. 1997a) and rebinned to match the dispersion of the CFHT spectra served as our template star. Differential spectroscopy, an example of which is depicted in Figure 4, produces EQWs quite compatible with those derived from IRAF Gaussian fits; thus, we are confident that template subtraction provided both accurate and precise line strength estimates. The paucity of suitable templates, however, forced us to rely, primarily, on the following method to estimate Be line strengths in stars where rotational broadening or poor S/N render standard measurement techniques useless.

3.1.3. *Profile Reconstruction*

Often the red feature of the Be resonance doublet was sufficiently blended with a strong blueward absorption line—a feature at 3130.8 Å attributed to a Ti II 3130.809 Å and Nb II 3130.780 Å blend—that standard EQW measurement techniques were incapable of accurately gauging the Be line strengths. In the absence of a suitable template spectrum, we attempted to "reconstruct" the 3131.064 Å Be line by subtracting the offending Ti + Nb blend, thereby revealing the blue side of the Be II feature. The EQW of the exposed Be absorption line was then determined using ordinary pixel summation or Gaussian fitting techniques. Figure 5 shows an example of this technique applied to the Be-weak star HR 244. The potential hazards of profile reconstruction are obvious: The possibility of attributing too much (or too little) flux to the Ti + Nb blend will necessarily affect the Be EQW measurement. The uncertainty associated with this procedure is accordingly somewhat larger than the error associated with more conventional line strength measurements. Consequently, we use this technique only when the all other methods fail.

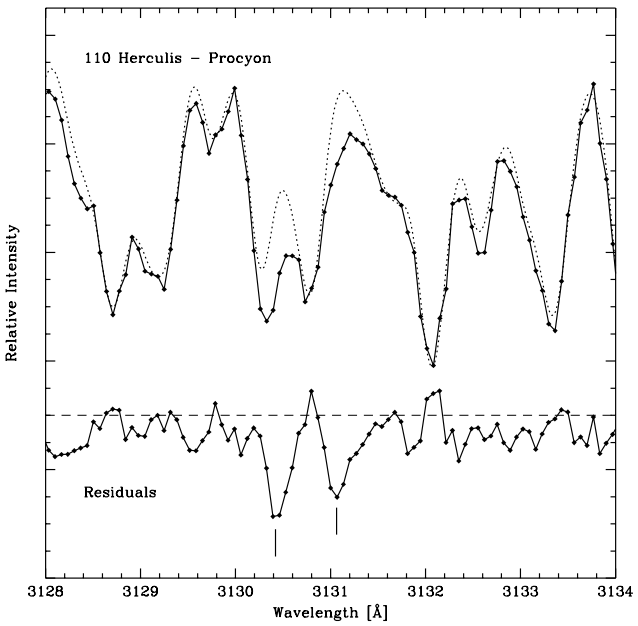

FIG. 4.—Differential spectroscopy example. The broadened, Be-poor template spectrum (Procyon, *dotted line*) is subtracted from the object spectrum HD 173667 (a.k.a. 110 Herculis, *solid line*). The resulting residuals, shown beneath the observed spectra, reveal the Be II resonance doublet of 110 Herculis.

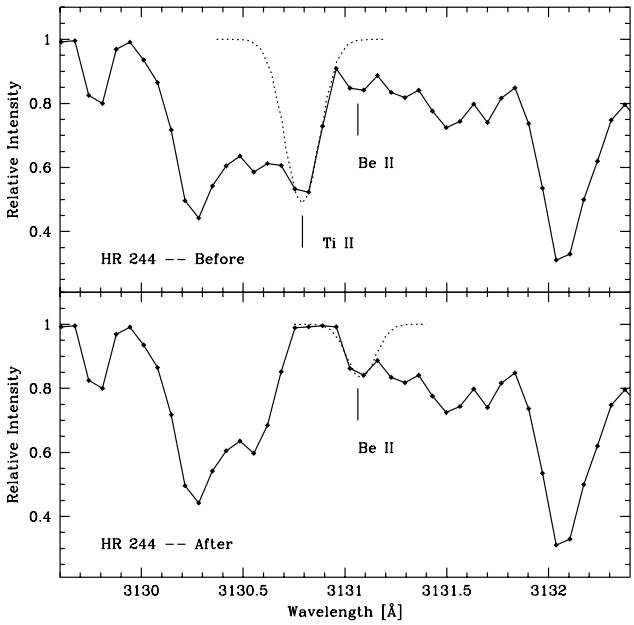

FIG. 5.—Example of profile reconstruction. (*top*) The Ti II + Nb II 3130.8 Å feature is fit with a Gaussian and subtracted from the spectrum of the Be-weak star HR 244. (*bottom*) This procedure reveals the "blue wall" of the 3131.064 Å Be absorption line, rendering it measurable with standard profile fitting routines.

3.1.4. *Error Estimates*

Photon-counting statistics and continuum placement ambiguity contribute to the uncertainty in measured EQWs. These error sources, however, were consistently dwarfed by the uncertainty in the fits used to estimate line strengths. Because IRAF fitting routines do not provide a unique fit to an absorption feature, the malleability of the fit can be used to "empirically" estimate the uncertainty in a measured EQW. Regardless of the technique used to *reveal* the 3131.064 Å line (see sixth column of Table 1), the EQW was, ultimately, measured using standard IRAF splot tasks. Thus, in all cases where the Be feature was detected, the degree of "flexibility" in the fitting function was used to estimate the smallest and largest acceptable fit. The EQWs listed in the fifth column of Table 1 therefore represent the "best-fit" line strengths while the 1 σ errors quoted in the seventh column of Table 1 reflect the empirically determined bounds of an adequate fit.

3.2. *Lithium*

Rather than use lithium abundance estimates from a variety of disparate sources, photospheric Li concentrations were calculated for our entire sample using published Li EQWs and stellar parameters identical to those involved in the Be abundance calculations (cf. § 4). We compiled a database of modern (circa 1981 and later) Li EQWs taken from the following sources: Lambert, Heath, & Edvardsson (1991), Balachandran (1990), Boesgaard, Budge, & Burck (1988), Pallavicini, Cerruti-Sola, & Duncan (1987), Hobbs & Duncan (1987), Boesgaard & Tripicco (1986b), Boesgaard & Lavery (1986), Rebolo, Molaro, & Beckman (1988), Spite & Spite (1982), and Duncan (1981). The Li line strengths listed in Table 1 represent a straight average of the literature values, but care was taken to excise potentially

erroneous EQWs from the calculation. More specifically, the uncertainty associated with the line strength measurements of Duncan (1981), leads us to exclude these estimates from the average if another published estimate exists. This is not an arbitrary exclusion of data, for the "photometric" technique used by Duncan (1981) produces Li EQWs that are, at times, much larger than modern spectroscopic measurements (Balachandran 1990). The average Li line strengths listed in Table 1 were used in all subsequent Li abundance calculations.

4. ABUNDANCE ANALYSIS

4.1. *Stellar Parameters*

The use of any abundance analysis methodology presupposes a knowledge of the basic observable properties of a star. These stellar parameters, which include effective temperature ($T_{\rm eff}$), surface gravity (log g), metal content ([Fe/H]), and the microturbulence velocity (ξ), are needed to select a model atmosphere that suitably matches the star under scrutiny. This model is subsequently used in the calculation of theoretical absorption features that estimate the number of absorbing Be atoms required to reproduce the observed line strengths. A sound estimate of the macroscopic properties of our program stars is of the utmost importance, so care was taken to ensure that systematic errors did not creep into the parameter calculations.

4.1.1. *Metallicities*

Two recent, homogeneous catalogs of cool dwarf metallicities (Taylor 1994b, 1995) served as the primary sources for the iron-to-hydrogen ratios listed in Table 2. Not all of the program stars were included in the Taylor references, so the catalog of Cayrel de Strobel et al. (1992) served as a backup. The tenth column of Table 2 lists the adopted metallicities.

4.1.2. *Effective Temperatures*

Numerous photometric effective temperature scales are present in the literature, and any one calibration may be fraught with hidden systematic errors. Therefore, in an attempt to avoid the precision errors associated with the use of one particular technique, we average several effective temperatures, computed using a variety of prescriptions, to arrive at our quoted surface temperature.

We utilized the Saxner & Hammarbäck (1985) $T_{\rm eff}$ calibrations based on Strömgren ($b-y$) and Hβ indices as well as their ($B-V$) calibration. Also incorporated were the Magain (1987) metallicity dependent ($b-y$) and ($B-V$) estimates. For stars with substantially sub–solar [Fe/H], we calculated $T_{\rm eff}$ using the King (1993) temperature scale. When available, we also used temperatures based on the Carney (1982) ($V-K$) calibration and infrared flux measurement techniques (Blackwell & Lynas-Gray 1994). Furthermore, we treat the ($R-I$) based temperatures compiled by Taylor (1994a, 1995) as valid $T_{\rm eff}$ estimates. All photometry used in the ($b-y$), ($B-V$), and Hβ calculations were taken from either the Hauck & Mermilliod (1990) catalog of Strömgren photometry or the Mermilliod & Mermilliod (1994) compilation of UBV data.

The mean effective temperatures listed in Table 3 are simply a straight average of the available $T_{\rm eff}$ estimates for a given star. The 1 σ $T_{\rm eff}$ errors, calculated using the standard deviation of the mean, ranged from 22 to 155 K with the average error being about 1%. We conservatively assume that this error represents the lowest possible uncertainty in the temperature calculation; therefore, we replaced errors smaller than 60 K with the mean in Table 3.

4.1.3. *Surface Gravities*

Beryllium abundances, whether they result from a CoG or spectrum synthesis analysis, are most sensitive to the adopted surface gravity (BK93; Garcia Lopez, Severino, & Gomez 1995; Kiselman 1994). We employ the gravity calculation described by Edvardsson et al. (1993, hereafter EAGLNT), which uses deviations in the Strömgren c_1 index and absolute visual magnitude from an empirically determined zero-age main-sequence (ZAMS) curve as a means of estimating log g. While only strictly valid for stars with H$\beta \in$ (2.58, 2.72), the EAGLNT formulation was used to determine log g for all program stars including HD 65583 (Hβ = 2.548) and HD 224930 (Hβ = 2.560). Extrapolation of the EAGLNT technique to include these stars provides a self-consistent estimate of the surface gravity for the entire sample.

Systematic errors in the c_1-Hβ sequence as well as random photometric errors contribute to the uncertainty in the log g calculation. Summing, in quadrature, the various error estimates delineated by EAGLNT results in a composite gravity uncertainty of roughly $\pm$0.20 dex. Several of our program stars are also part of the EAGLNT study, and, although we use a different $T_{\rm eff}$ calibration, our surface gravities are consistent with EAGLNT's to within $\pm$0.05 dex. Despite the general agreement, we adopt 0.20 dex as a safe estimate of the uncertainty in a computed surface gravity.

4.1.4. *Microturbulence Parameter*

BK93 demonstrate that Be abundances calculated from weak lines are unaffected by the choice of ξ, while abundances estimated using lines with large ($\geq$80 mÅ) EQWs are dependent, albeit only slightly, upon the chosen microturbulent velocity. The uncertainty introduced by minor ($\sim$0.5 km s^{-1}) changes in ξ, however, is small when compared to the effect EQW or log g errors have on the calculated Be abundances. Li abundances, too, are only mildly affected by the choice of ξ (Balachandran 1990). We therefore use the mean of the sample (1.5 km s^{-1}—calculated using the Nissen 1981 formulation) as the characteristic turbulent velocity in all abundance calculations.

4.2. *Abundances*

4.2.1. *Beryllium*

The assumption that local processes govern the formation of spectral features greatly simplifies any attempt to assay the chemical content of a stellar photosphere. Invoking the condition that local thermodynamic equilibrium (LTE) determine the relative population of atomic levels is, however, not always valid. In particular, the resonance doublet of Be II forms in a region affected by distinctly nonlocal phenomena. (Kiselman & Carlsson 1995; Garcia Lopéz, Severino, & Gomez 1995). Kiselman & Carlsson (1995) note that Be I atoms are bathed in a hot UV radiation field and consequently suffer overionization; furthermore, bound-bound pumping tends to overexcite Be II, depopulating the ground state of this ion. While the former

TABLE 2

STELLAR PHOTOMETRY AND METALLICITIES

HD Number	HR Number	MK Type	$(b-y)$[a]	m_1[a]	c_1[a]	Hβ[a]	$(B-V)$[b]	$(V-K)$[c]	[Fe/H]	Reference
4614	219	G0 V	0.372	0.185	0.275	2.588	0.57	...	−0.24	2
4813	235	F7 IV–V	0.334	0.156	0.366	2.625	0.51	...	−0.14	1
5015	244	F8 V	0.346	0.193	0.412	2.613	0.54	...	+0.02	1
10307	483	G1.5 V	0.389	0.203	0.338	2.604	0.62	...	+0.00	1
13555	646	F5 V	0.308	0.132	0.466	2.647	0.43	...	−0.29	2
19994	962	F8 V	0.361	0.183	0.424	2.630	0.57	...	+0.15	2
30649	...	G1 IV–V	0.386	0.157	0.297	2.581	0.59	...	−0.46	1
34411	1729	G2 IV–V	0.389	0.206	0.363	2.598	0.63	...	+0.16	1
61421	2943	F5 IV–V	0.272	0.167	0.532	2.671	0.42	...	−0.02	1
64096	3064	G0 V	0.378	0.202	0.318	2.622	0.60	...	−0.06	1
65583	...	G8 V	0.449	0.234	0.231	2.548	0.71	...	−0.54	1
90508	4098	F9 V	0.397	0.177	0.295	2.579	0.60	1.52	−0.48	1
101606	4501	F4 V	0.312	0.118	0.401	2.630	0.44	1.16	−0.82	3
106516	4657	F5 V	0.318	0.115	0.332	2.613	0.47	1.25	−0.67	1
110897	4845	G0 V	0.374	0.149	0.284	2.578	0.55	1.45	−0.46	2
113022	4926	F6 V	0.292	0.172	0.455	2.660	0.42	...	+0.09	1
114762	...	F9 V	0.363	0.128	0.295	2.590	0.53	...	−0.66	2
117176	5072	G2 V	0.446	0.232	0.351	2.576	0.71	...	−0.04	1
119288	5156	F3 V	0.278	0.144	0.463	2.662	0.41	...	−0.20	3
126141	5387	F5 V	0.261	0.161	0.488	2.685	0.37	...	+0.00	3
128093	5445	F5 V	0.300	0.131	0.476	2.657	0.40	...	−0.11	3
128167	5447	F2 V	0.253	0.132	0.489	2.681	0.36	0.97	−0.39	1
128429	5455	F5 V	0.310	0.146	0.434	2.637	0.46	...	−0.22	3
130817	5529	F2 V	0.258	0.139	0.518	2.678	0.36	...	−0.39	3
142373	5914	F8 V	0.380	0.153	0.325	2.601	0.56	1.47	−0.43	1
145976	6052	F3 V	0.252	0.161	0.559	2.685	0.38	...	+0.01	3
146233	6060	G2 V	0.398	0.221	0.341	2.592	0.65	...	+0.04	1
148816	...	F9 V	0.365	0.125	0.308	2.588	0.54	1.42	−0.69	2
150177	6189	F3 V	0.330	0.123	0.395	2.613	0.49	...	−0.63	2
154417	6349	F8.5 IV–V	0.363	0.190	0.327	2.604	0.58	...	+0.10	1
156897	6445	F2 V	0.253	0.149	0.501	2.680	0.39	...	−0.16	3
157089	...	F9 V	0.379	0.145	0.327	2.588	0.58	1.49	−0.58	1
157214	6458	G0 V	0.409	0.182	0.309	2.589	0.62	1.54	−0.39	2
157373	6467	F4 V	0.291	0.121	0.444	2.652	0.41	...	−0.43	1
159332	6541	F6 V	0.328	0.148	0.471	2.631	0.49	...	−0.22	2
160693	...	G0 V	0.382	0.144	0.295	2.577	0.58	1.51	−0.57	1
161023	6600	F0 V	0.253	0.137	0.516	2.684	0.38	...	−0.17	3
165908	6775	F7 V	0.356	0.135	0.324	2.609	0.51	1.43	−0.47	2
166285	6797	F5 V	0.310	0.152	0.451	2.642	0.45	...	−0.22	3
168151	6850	F5 V	0.281	0.143	0.472	2.653	0.40	...	−0.37	2
173667	7061	F6 V	0.314	0.150	0.484	2.648	0.46	...	−0.08	1
182101	7354	F6 V	0.309	0.137	0.424	2.644	0.45	...	−0.19	3
184499	...	G0 V	0.391	0.143	0.313	2.579	0.58	1.34	−0.75	1
185395	7469	F4 V	0.261	0.158	0.506	2.689	0.38	...	+0.01	1
191195	7697	F5 V	0.280	0.156	0.507	2.679	0.41	...	+0.01	1
192455	7727	F5 V	0.334	0.186	0.464	2.633	0.47	...	+0.00	3
192985	7756	F5 V	0.281	0.164	0.481	2.671	0.40	...	−0.03	1
195633	...	G0 V	0.363	0.118	0.369	2.607	0.52	...	−1.00	3
198390	7973	F5 V	0.302	0.136	0.419	2.652	0.43	...	−0.22	3
200790	8077	F8 V	0.346	0.171	0.423	2.624	0.54	...	−0.07	1
204121	8205	F5 V	0.298	0.165	0.478	2.662	0.45	...	+0.06	1
207978	8354	F6 IV–V	0.301	0.116	0.426	2.640	0.41	1.17	−0.62	2
208906	...	F8 IV–V	0.345	0.121	0.282	2.599	0.50	1.35	−0.73	2
211976	8514	F6 V	0.299	0.147	0.422	2.626	0.45	...	−0.39	3
218470	8805	F5 V	0.286	0.152	0.495	2.672	0.42	...	−0.15	2
220117	8885	F5 V	0.296	0.170	0.489	2.663	0.46	...	−0.02	2
222368	8969	F7 V	0.329	0.164	0.395	2.622	0.51	...	−0.13	1
224930	9088	G2 V	0.428	0.189	0.215	2.560	0.67	1.88	−0.65	1
225239	9107	G2 V	0.412	0.169	0.312	2.592	0.62	1.67	−0.44	1

[a] Strömgren photometry from Hauck & Mermilliod 1990.
[b] $(B-V)$ data from Mermilliod & Mermilliod 1994.
[c] $(V-K)$ data from Carney 1982.
REFERENCES.—(1) Taylor 1994b; (2) Taylor 1995; (3) Cayrel de Strobel et al. 1992.

nonlocal effect strengthens the 3131.064 Å line, by populating the ground state of singly ionized Be, the latter reduces the Be II line opacity by removing potential absorbers from the lower energy level (Garcia Lopéz et al. 1995). The increase in the 3131.064 Å line strength due to overionization is roughly balanced by the line dilution of overexcitation; thus, the non-LTE (NLTE) effects negate one another, resulting in an absorption feature that appears to have formed in an environment characterized by LTE. It is this fortunate cancellation of NLTE effects that ultimately justifies the use of LTE spectral analysis routines in the calculation of Be abundances.

TABLE 3
EFFECTIVE TEMPERATURES

HD Number	HR Number	$(B-V)$[a]	$(b-y)$[a]	Hβ[a]	$(B-V)$[b]	$(b-y)$[b]	$(b-y)$[c]	$(V-K)$[d]	IRFM[e]	$(R-I)$[f]	$T_{\rm eff}$	$\sigma(T_{\rm eff})$
4614	219	5928	5889	5738	5821	5860	...	...	6044	5902	5883	95
4813	235	6188	6157	6137	6110	6147	...	...	...	6131	6145	60
5015	244	6138	6118	6010	6150	6145	...	...	...	6102	6111	60
10307	483	5844	5842	5914	5858	5860	...	...	...	5854	5862	60
13555	646	6438	6292	6362	6321	6272	...	...	...	6308	6332	60
19994	962	6084	6056	6189	6230	6142	...	...	...	6094	6133	67
30649	...	5764	5742	...	5632	5707	...	...	...	5734	5716	60
34411	1729	5879	5885	5848	6065	5981	...	...	5947	5909	5931	74
61421	2943	6557	6576	6600	6524	6598	...	...	...	6528	6564	60
64096	3064	5892	5897	6105	5864	5899	...	...	...	5986	5941	91
65583	...	...	...	...	...	5259	...	...	...	5396	5328	97
90508	4098	5715	5663	...	5583	5627	5687	5686	...	5695	5665	60
101606	4501	...	...	6189	6146	6166	6254	6314	...	...	6214	69
106516	4657	...	...	6010	6049	6139	6214	6154	...	6109	6112	74
110897	4845	5918	5821	...	5788	5787	...	5798	...	5867	5830	60
113022	4926	6588	6471	6492	6619	6525	...	...	...	6478	6529	62
114762	...	...	...	...	5808	5830	5914	...	...	5909	5865	60
117176	5072	...	...	...	...	...	...	...	5488	5588	5538	70
119288	5156	6540	6504	6512	6439	6495	...	...	...	...	6498	60
126141	5387	6740	6648	6734	6704	6674	...	...	...	...	6700	60
128093	5445	6602	6381	6462	6526	6380	...	...	...	...	6470	96
128167	5447	6678	6632	6696	6555	6621	...	6705	6763	6545	6650	76
128429	5455	6347	6294	6261	6243	6278	...	...	...	...	6285	60
130817	5529	6678	6599	6667	6554	6587	...	...	...	...	6617	60
142373	5914	5891	5789	5881	5760	5753	...	5766	...	5767	5801	60
145976	6052	6707	6707	6734	6678	6736	...	...	...	...	6712	60
146233	6060	...	5798	...	...	5835	...	...	...	5793	5809	60
148816	...	...	...	...	5760	5812	5900	5848	...	5847	5833	60
150177	6189	...	...	6010	...	6061	6134	...	...	6029	6058	60
154417	6349	6029	6031	5914	6125	6092	...	...	...	5979	6028	76
156897	6445	6625	6671	6686	6533	6671	...	...	...	...	6637	63
157089	...	...	...	...	5629	5732	5807	5733	...	5793	5739	70
157214	6458	5677	...	...	5547	5568	5607	5655	...	5657	5618	60
157373	6467	6473	6375	6413	6347	6357	...	...	...	6380	6391	60
159332	6541	6235	6178	6199	6132	6159	...	...	...	6169	6179	60
160693	...	...	...	...	5630	5712	5787	5702	...	5676	5701	60
161023	6600	6659	6669	6725	6564	6668	...	...	...	...	6657	60
165908	6775	6073	5938	5967	5944	5909	...	5831	...	6022	5955	78
166285	6797	6385	6294	6312	6280	6278	...	...	...	...	6310	60
168151	6850	6529	6452	6423	6406	6435	...	...	...	6340	6431	62
173667	7061	6392	6297	6372	6333	6301	...	...	6380	6396	6353	60
182101	7354	6394	6307	6332	6297	6294	...	...	...	...	6325	60
184499	...	...	...	...	5587	5626	5727	5984	...	5701	5725	155
185395	7469	6707	6650	6772	6677	6678	...	...	6713	6684	6697	60
191195	7697	6599	6530	6677	6574	6557	...	...	...	6588	6588	60
192455	7727	6382	6189	6220	6367	6211	...	...	...	...	6274	93
192985	7756	6625	6517	6600	6582	6536	...	...	...	6554	6569	60
195633	...	...	...	5946	5795	5800	5914	...	...	...	5864	78
198390	7973	6459	6345	6413	6355	6331	...	...	...	...	6380	60
200790	8077	6107	6098	6126	6066	6101	...	...	...	6072	6095	60
204121	8205	6472	6427	6512	6489	6469	...	...	...	6429	6466	60
207978	8354	...	...	6292	6300	6261	6327	6295	...	6238	6285	60
208906	...	...	...	5859	5915	5946	6034	5966	...	5922	5940	60
211976	8514	6331	6330	6147	6205	6310	6341	...	...	...	6277	81
218470	8805	6518	6463	6609	6432	6459	...	...	...	6486	6494	63
220117	8885	6413	6425	6522	6388	6445	...	...	...	6429	6437	60
222368	8969	6194	6192	6105	6121	6185	...	...	...	6124	6154	60
224930	9088	...	...	...	...	5384	5480	5171	...	5472	5377	144
225239	9107	5654	...	...	5522	5534	...	5460	...	5701	5574	100

[a] Saxner & Hammarbäch 1985.
[b] Magain 1987.
[c] King 1993.
[d] Carney 1982.
[e] Blackwell & Lynas-Gray 1994.
[f] Taylor 1994a, 1995.

Photospheric beryllium abundances [N(Be)][4] were estimated using Kurucz (1992, private communication) atmospheres in conjunction with MOOG, an LTE spectral line analysis package (Sneden 1973). The Kurucz model atmospheres blanket the space of temperature, gravity, and metallicity appropriate to F and G dwarfs. By interpolating within the $T_{\rm eff}$, log g, and [M/H] lattice, we tailored individual model atmospheres to match the gross physical proper-

[4] Throughout we use the abundance terminology $N(X)$, which represents the logarithm of abundance by number of an element X, or $N(X) = \log(X/{\rm H}) + 12$, relative to hydrogen.

ties of each program star. Given an observed equivalent width, MOOG can calculate, for a specific stellar model, the elemental abundance required to produce a theoretical absorption feature with an identical line strength. Moreover, the line can be treated as a single feature or a blend. Because the 3131.064 Å line does not reside in a sparsely populated region of wavelength space, we model the Be II feature as a blend of both molecular and metallic absorption lines. Atomic data for a $\sim$0.1 Å window centered on the red Be II resonance line were extracted from the Kurucz (1993) CD-ROM. Alterations to this line list include a reduction in the oscillator strength of a CH (3131.058 Å) feature identical to the one employed by King, Deliyannis, & Boesgaard (1997) and an enhancement in the *gf* value of a Mn II line centered on 3131.015 Å. The increase in the Mn II oscillator strength (0.82 dex), while not as large as that required to match the spectra of the solar analogs modeled by King et al. (1997), provided an adequate synthetic spectrum fit (see below) to several of our high-resolution GECKO spectra. Beryllium abundances calculated using the adjusted line list and the aforementioned line strength force-fitting method are listed in the seventh column of Table 4.

Errors in the measured equivalent widths, rather than uncertainties in any one of the calculated stellar parameters, are the primary source of uncertainty in the presented Be abundances. On average, the empirically determined EQW errors translated into an N(Be) uncertainty of 0.18 dex. This measurement error dominates over its nearest competitors, namely propagation of gravity and temperature uncertainties. For the Be II blend, a 0.2 dex change in the surface gravity translates roughly into a 0.1 dex uncertainty in N(Be), while a 100 K deviation in the effective temperature typically results in a 0.05 dex change in the Be abundance. Propagated metallicity errors were negligible. The adopted 1 σ uncertainty in the Be abundances listed in the eighth column of Table 4 reflect a sum, in quadrature, of the EQW, log g, and $T_{\rm eff}$ errors. Recent, observations of HR 4501 (Boesgaard et al. 1998b) confirm speckle observations (Bonneau et al. 1986; Blazit, Bonneau, & Foy 1987) that this object is actually a binary system. Consequently, the adopted Be (and Li) upper limits are, most likely, too small since flux dilution by the companion was not taken into account.

Spectrum synthesis, while not the focus of this study, was performed on several high resolution spectra obtained during the 1995 October CFHT observing run. An expansive list of $\sim$200 absorption features that inhabit a 3 Å window centered on the Be II region (King et al. 1997) served as MOOG input as did model atmospheres interpolated from the Kurucz (1992, private communication) $T_{\rm eff}$, log g, and [M/H] grid. Apart from altering the 3131.058 Å CH and 3131.015 Å Mn II oscillator strengths, a few, largely cosmetic, changes were made to the King et al. (1997) line list, but these modifications did not significantly affect the derived Be abundances. The calculated artificial spectra, examples of which are shown in Figure 6, have Be abundances adjusted to fit the Be II 3131.064 Å feature. The model spectra not only match the observed GECKO spectra but the "dialed-in" Be abundances, listed in Table 5, are also entirely consistent with the N(Be) values calculated using the MOOG line strength force fit. The general agreement between the two independent analysis methods suggests that the most error-prone procedure (line strength force fitting) does, in fact, produce reliable photospheric abundances. The only noticeable difference between the two techniques is that spectrum synthesis abundances tend to be smaller than EQW based abundances. The measured line strengths, however, could possibly overestimate the strength of the Be II blend, resulting in the small systematic differences observed here. Thus, the Be abundance trends, based primarily on the EQW analysis, may *underestimate*, albeit slightly, the severity of Be depletion in our sample.

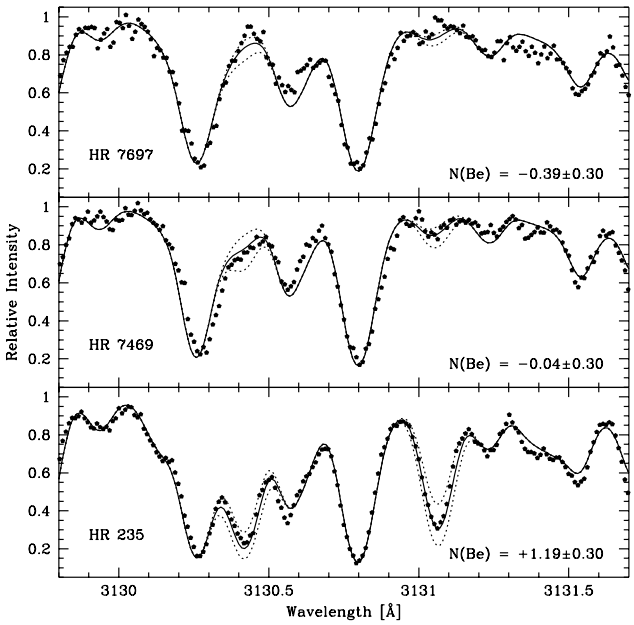

FIG. 6.—Three examples of spectrum syntheses (*lines*) superimposed upon GECKO data (*solid pentagons*). Solid lines denote the "best" synthetic spectrum fit to each observed spectrum. Dotted lines denote $\pm$0.30 dex deviations in the best-fit Be abundance and typify the uncertainty in a given abundance. The adopted Be concentrations for the stars HR 235, HR 7469, and HR 7697 are 1.19, −0.04, and −0.39 dex, respectively.

4.2.2. *Lithium*

Li abundances were determined using Li EQW averages, MOOG, and the stellar parameters listed in Table 4. We assumed that the measured Li line strengths could be modeled as simple blend consisting of the Li resonance doublet ($\lambda \sim 6707.8$ Å) split by the hyperfine interaction and a neutral iron line ($\lambda \sim 6707.411$ Å). All atomic data for the Li blend were taken from Andersen, Gustafsson, & Lambert (1984). Exploring the sensitivity of the Li abundance calculation to the input parameters, we find that a 100 K change in $T_{\rm eff}$ translates into the largest abundance uncertainty. On average, a variation of 100 K leads approximately to a 0.09 dex change in the Li abundance. Non-LTE corrections also deserve consideration. The analysis of Carlsson et al. (1994) shows, however, that NLTE abundance corrections are small. On average, NLTE Li abundances differed from those calculated assuming LTE by a mere 0.03 dex. Because temperature and NLTE errors are the dominant sources of uncertainty in the Li calculations, we adopt 0.10 dex, the quadrature sum of σ_{T_e} and $\sigma_{\rm NLTE}$, as the 1 σ error in the revised abundances.

5. DISCUSSION

The light elements are excellent tracers of the physics operating beneath the surface of otherwise ordinary F and

TABLE 4

CALCULATED STELLAR PARAMETERS AND ABUNDANCES

HD Number	HR Number	log (g)	$T_{\rm eff}$	ξ	N(Li)	N(Be)	σN(Be)
4614	219	4.49	5883	1.10	+1.90	+1.19	0.26
4813	235	4.36	6145	1.36	+2.76	+1.22	0.16
5015	244	3.99	6111	1.83	< +0.31	+0.11	0.16
10307	483	4.32	5862	1.33	< +1.85	+1.16	0.19
13555	646	4.09	6332	1.77	+2.96	+0.95	0.18
19994	962	4.12	6133	1.67	+2.09	+1.11	0.19
30649	...	4.27	5716	1.34	+1.71	+0.86	0.13
34411	1729	4.11	5931	1.62	< +1.76	+1.12	0.21
61421	2943	4.04	6564	1.91	< +0.78	< −1.21	...
64096	3064	4.57	5941	1.03	+2.04	+1.47	0.20
65583	...	4.47	5328	0.96	< +0.94	+0.80	0.22
90508	4098	4.30	5665	1.28	n/a	+1.00	0.27
101606	4501	4.18	6214	1.62	< +1.09	< −0.52	...
106516	4657	4.33	6112	1.40	< +1.46	< −0.61	...
110897	4845	4.27	5830	1.37	+1.87	+1.06	0.26
113022	4926	4.24	6529	1.64	< +1.83	< +0.09	...
114762	...	4.31	5865	1.33	+1.94	+0.95	0.33
117176	5072	4.02	5538	1.61	+1.79	+0.86	0.22
119288	5156	4.26	6498	1.60	< +1.03	< −0.10	...
126141	5387	4.35	6700	1.55	< +1.81	+0.86	0.25
128093	5445	4.14	6470	1.75	< +1.28	< −0.05	...
128167	5447	4.31	6650	1.58	< +1.74	< −0.66	...
128429	5455	4.14	6285	1.69	< +1.51	< +0.07	...
130817	5529	4.19	6617	1.74	< +1.31	< +0.24	...
142373	5914	4.34	5801	1.27	+2.36	+1.27	0.20
145976	6052	4.08	6712	1.90	+2.82	+0.48	0.31
146233	6060	4.18	5809	1.49	+1.58	+1.16	0.36
148816	...	4.22	5833	1.44	+1.84	+0.90	0.18
150177	6189	4.03	6058	1.76	+2.41	+0.72	0.14
154417	6349	4.35	6028	1.33	+2.74	+1.13	0.26
156897	6445	4.28	6637	1.63	< +1.81	< +0.40	...
157089	...	4.17	5739	1.48	+1.87	+1.03	0.15
157214	6458	4.37	5618	1.18	< +0.65	+0.74	0.18
157373	6467	4.22	6391	1.63	< +1.54	< −0.17	...
159332	6541	3.92	6179	1.95	< +1.53	+0.17	0.28
160693	...	4.22	5701	1.41	< +1.14	+0.42	0.22
161023	6600	4.25	6657	1.67	< +1.51	< −0.26	...
165908	6775	4.38	5955	1.27	+2.31	+0.93	0.12
166285	6797	4.12	6310	1.72	< +1.65	−0.14	0.26
168151	6850	4.13	6431	1.75	< +1.39	+0.28	0.21
173667	7061	4.04	6353	1.85	+1.64	+0.36	0.13
182101	7354	4.25	6325	1.56	+1.73	+0.68	0.13
184499	...	4.13	5725	1.52	+1.41	+0.68	0.26
185395	7469	4.33	6697	1.58	< +0.34	−0.11	0.26
191195	7697	4.24	6588	1.66	+1.70	< −1.28	...
192455	7727	3.93	6274	1.96	< +1.63	< −0.41	...
192985	7756	4.25	6569	1.64	< +1.55	< −1.23	...
195633	...	4.12	5864	1.59	+2.29	+0.71	0.18
198390	7973	4.35	6380	1.45	+2.33	+0.97	0.18
200790	8077	4.08	6095	1.71	< +0.99	−0.15	0.24
204121	8205	4.18	6466	1.70	+2.35	+0.46	0.17
207978	8354	4.17	6285	1.66	< +1.69	< −0.38	...
208906	...	4.46	5940	1.16	+2.39	+0.81	0.17
211976	8514	4.07	6277	1.78	+2.33	+0.94	0.18
218470	8805	4.23	6494	1.64	< +1.68	< +0.07	...
220117	8885	4.15	6437	1.73	+1.57	+0.79	0.23
222368	8969	4.19	6154	1.59	+2.20	+1.04	0.18
224930	9088	4.62	5377	0.78	< +0.68	+0.98	0.16
225239	9107	4.37	5574	1.16	+1.86	+1.34	0.15

G stars; however, relating an observed abundance to a physical process rests fundamentally upon one basic assumption: that the initial Be (or Li) abundance is known. Unfortunately, a collection of field stars that span a wide range of metallicities, such as those presented here, form an inhomogeneous group without a common age, dynamical, or chemical history. Assigning a unique initial, or cosmic, abundance to the entire sample may be difficult. However, breaking the sample into reasonably cohesive subgroups that possibly share common histories and properties does, at least, facilitate the exploration of correlations between light element abundances and other, fundamental stellar parameters. We therefore segregate our sample into two groups: "solar metallicity" ([Fe/H] ≥ -0.5) and "intermediate metallicity" ($-1.0 \leq$ [Fe/H] < -0.5) stars. While this dividing line is somewhat arbitrary, dis-

TABLE 5

CURVE OF GROWTH AND SPECTRUM SYNTHESIS ABUNDANCES

HD Number	HR Number	$N(\mathrm{Be})_{\mathrm{CoG}}$	$\sigma N(\mathrm{Be})_{\mathrm{CoG}}$	$N(\mathrm{Be})_{\mathrm{SYN}}$	$\sigma N(\mathrm{Be})_{\mathrm{SYN}}$
4614.....	219	+1.19	0.26	+1.17	0.30
4813.....	235	+1.22	0.16	+1.19	0.30
13555.....	646	+0.95	0.18	+0.81	0.30
173667.....	7061	+0.36	0.13	+0.33	0.30
182101.....	7354	+0.68	0.13	+0.66	0.30
185395.....	7469	−0.11	0.26	−0.04	0.30
191195.....	7697	< -1.28	...	$\ll -0.39$	...
200790.....	8077	−0.15	0.24	−0.09	0.30
218470.....	8805	$< +0.07$	...	< -0.31	...
220177.....	8885	+0.79	0.23	+0.56	0.30

tinguishing between Population I (solar [Fe/H]) and intermediate Population I (intermediate [Fe/H]) stars hopefully reduces the likelihood that differential galactochemical or evolutionary effects will either obscure or distort abundance trends.

At once present during and separated from the formation of the sun, carbonaceous chondrite meteorites, fossils of the ancient interstellar medium (ISM), reflect the chemical makeup of the primitive solar system. Assaying the composition of these old rocky bodies provides an estimate of the Li and Be content of the nascent solar nebula. Despite the complications that chemical fractionation effects may have on meteoritic abundance analyses, we use lithium [$N(\mathrm{Li}) = 3.31 \pm 0.04$] and beryllium [$N(\mathrm{Be}) = 1.42 \pm 0.04$] abundances extracted from carbonaceous chondrites (Anders & Grevesse 1989) as plausible cosmic values. It is reassuring that F stars in the youngest open clusters appear to have photospheric Li abundances consistent with the protosolar value. The average value of $N(\mathrm{Li})$ for α Per stars hotter than 6000 K (age $\approx 5 \times 10^7$ yr) is 3.21 ± 0.16 (Balachandran, Lambert, & Stauffer 1988). Pleiades F dwarfs (age $\approx 7 \times 10^7$ yr) also exhibit a large mean Li abundance [$N(\mathrm{Li}) = 3.06 \pm 0.14$] (Soderblom et al. 1993). Thus, we are confident the meteoritic Li reflects the initial abundance of our solar metallicity stars.

The working hypothesis of this paper is that stars which deplete Li may also deplete Be. Therefore, only Li-rich stars should retain an undepleted supply of Be. However, few cluster or field stars with near meteoritic Li levels have simultaneous Be measurements. The field star HR 3775 has an undepleted Li abundance, $N(\mathrm{Li}) = 3.25$ (average of Lambert et al. 1991 and Balachandran 1990) and a near meteoritic Be of 1.40 (average of Boesgaard 1976; Boesgaard & Chesley 1976; BK93; Boesgaard et al. 1998b) suggesting that our choice of initial Be is plausible. Furthermore, stars from BK93 that have modest Li deficiencies ($N(\mathrm{Li}) \in [2.5, 3.3]$—excluding the binary HR 8430) and are not part of this survey have a mean Be abundance of 1.35, which is within 2 standard deviations of the meteoritic abundance. It is possible, though, that the meteoritic Be abundance slightly overestimates the cosmic level. Previous studies (Boesgaard 1976) found the average Be abundance in F and G dwarfs to be ~ 1.11. More observations of Be in Li-normal stars are needed to settle the issue of the cosmic Be abundance. Although we assume that our solar metallicity stars, objects that likely formed from gas clouds chemically similar to the protosolar nebula, initially contained meteoritic concentrations of the light elements, we also note that this issue is unresolved and stars may have arrived on the ZAMS with a Be abundance as low as the value quoted by Boesgaard (1976).

The initial abundances for the intermediate metallicity stars are more problematical. For Be, the $N(\mathrm{Be})$ versus [Fe/H] (Boesgaard 1996) relation may be used as a guide, and we assume the galactic evolution of Be can constrain the range of possible Be values for intermediate metallicity stars. Using Figure 8 of Boesgaard (1996), we estimate $N(\mathrm{Be})_{\mathrm{init}}$ may range from 0.9 dex to near meteoritic levels (≈ 1.4 dex) in our intermediate Population sample. For Li, the issue is considerably more complicated, as we now outline. Of the light element tracers, Li is the most fragile and is considerably more susceptible to destruction than Be (or B). Li is also the heaviest element produced in relevant amounts during the epoch of big bang nucleosynthesis. For some baryonic densities in standard (homogeneous) nucleosynthesis, and for much of the parameter space in inhomogeneous models, the primordial Li (Li_p) could be as high as the meteoritic value, roughly an order of magnitude above the observed level of the halo Li plateau ($N(\mathrm{Li}) \sim 2.2$—Bonifacio & Molaro 1997). This would require that halo stars have depleted their Li by an order of magnitude over their lifetime. Conversely, in standard nucleosynthesis Li_p could be as low as the halo plateau. This would require Galactic Li enrichment to raise the Li abundance to the meteoritic level, the value observed in young open clusters. In summary, the precise value of Li_p is not known with great confidence but is likely to be somewhere between 2.2 and 3.3. Since we have no means of constraining the initial Li abundance for our intermediate [Fe/H] stars, we simply note that the cosmic level lies somewhere between the halo plateau and the meteoritic abundance.

Figures 7*a* and 7*b* show the updated Li and newly calculated Be abundances for our sample of solar and intermediate metallicity stars as a function of effective temperature. In each figure, unambiguous detections are represented by solid pentagons, while solid inverted triangles denote upper limits. The dashed horizontal lines represent the adopted initial abundance (or abundance spread) appropriate for both that particular species and metallicity class. These diagrams immediately reveal our selection bias: Our stars are predominantly Li-deficient. Lithium abundances in these solar metallicity stars vary from 0.3–2.0 dex below cosmic levels at all temperatures above 6000 K, while below 6000 K the largest detectable Li abundance steadily declines from 2.5 dex at 6000 K to 1.9 dex at 5500 K.

While the Li data shows little correlation with T_{eff}, several distinct trends in the $N(\mathrm{Be})$-T_{eff} plane are readily apparent. Solar metallicity stars with temperatures in excess of 6100 K exhibit a wide range of Be values, but all of these warm, Li-poor stars appear to be significantly Be-deficient with respect to the meteoritic level. No star within this temperature window possesses more than $\sim 40\%$ of its initial Be, and stars that retain only 2% of its initial Be allotment are quite common. A depletion maximum (or abundance minimum) occurs near 6500 K, corresponding to the red wing of the Li gap in Population I open cluster stars. This abundance dip is likely the Be analog to the Boesgaard gap; however, as is the case for the field star Li data, any tight correlation between Be abundance and effective temperature is washed out by age, chemical, or evolutionary differences in this sample of unrelated stars. Nevertheless, it

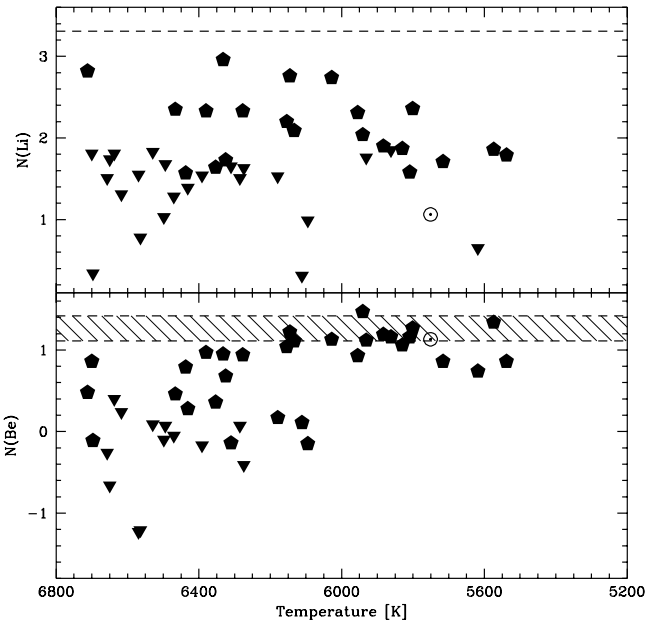

FIG. 7*a*

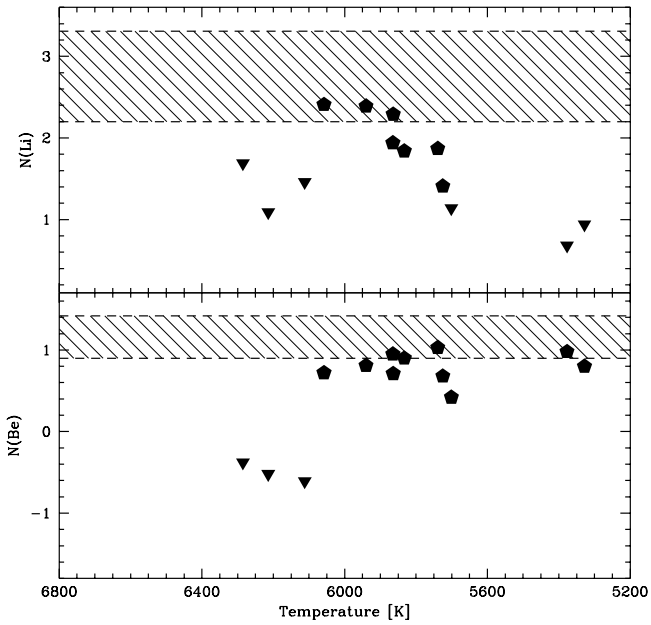

FIG. 7*b*

FIG. 7.—(*a*) Lithium and beryllium abundances for the solar metallicity sample ([Fe/H] ≥ -0.5) are plotted vs. effective temperature. Pentagons represent detections, while inverted triangles denote abundance upper limits. Shaded regions bordered by dashed horizontal lines reveal the plausible range of initial abundances for each element in this metallicity bin. While there is little question the meteoritic Li abundance equals the initial abundance for solar metallicity stars [$N(\mathrm{Li})_{\mathrm{met}} = N(\mathrm{Li})_{\mathrm{init}} = 3.31$], it is possible that the initial Be abundance could be as high as 1.42 (meteoritic) or as low as 1.11 (Boesgaard 1976). (*b*) Same as (*a*) except the intermediate metallicity data ($-1.0 \leq$ [Fe/H] ≤ -0.5) are shown. There is a great deal of ambiguity in both the initial Li and Be abundances for this subsample. We use the upper envelope of the Boesgaard (1996) N(Be) vs. T_{eff} relationship to estimate likely upper ($\sim$1.4 dex) and lower ($\sim$0.9 dex) initial Be abundances. However, since Li is both easily destroyed (in stellar interiors) and produced in copious amounts (in most models of big bang nucleosynthesis), the galactic evolution of Li with [Fe/H] does not provide a convenient means of constraining $N(\mathrm{Li})_{\mathrm{init}}$. Therefore, the Li abundances seen in halo stars [N(Li) $\approx$ 2.2] and meteorites [N(Li) $\approx$ 3.3] serve as the lower and upper estimates of the initial Li concentration for the intermediate metallicity stars.

is evident that stars which significantly deplete their Li reserves by factors of 10–100 may also be significantly Be-deficient. Figure 8, a plot of N(Be) versus N(Li), reveals that a solar metallicity star which preserves more than 10% of its initial lithium retains roughly 30%, or more, of its original Be. However, stars with stronger Li deficiencies *may* exhibit significant Be depletion. In other words, the stars that are the most Be-poor are also severely Li-deficient, as one might expect given the relative depths of the Li and Be nuclear destruction zones. This trend is also recognizable in our intermediate metallicity stars, although poor statistics and ambiguity in the initial abundance makes such assertions tenuous. Unlike the warm F-dwarfs, cool ($T_{\mathrm{eff}} < 6100$ K) Li-deficient stars presented here do not appear to be significantly Be-poor. The measured abundances in the cool, solar [Fe/H] stars are *at most* depleted by a factor of $\approx$4 with respect to the meteoritic level.

The data reveal that warm stars which populate the effective temperature regime typically associated with the Li abundance gap also exhibit significant Be deficiencies. However, cooler stars retain a large majority of their initial Be. Thus, stars that, by some process, actively destroy or hide their initial Li reserve also appear to have a dwindling supply of Be. As we shall see, these abundance trends provide a useful discriminant when attempting to isolate which hypothesized physical process removes the light elements from the atmospheres of cool main-sequence stars.

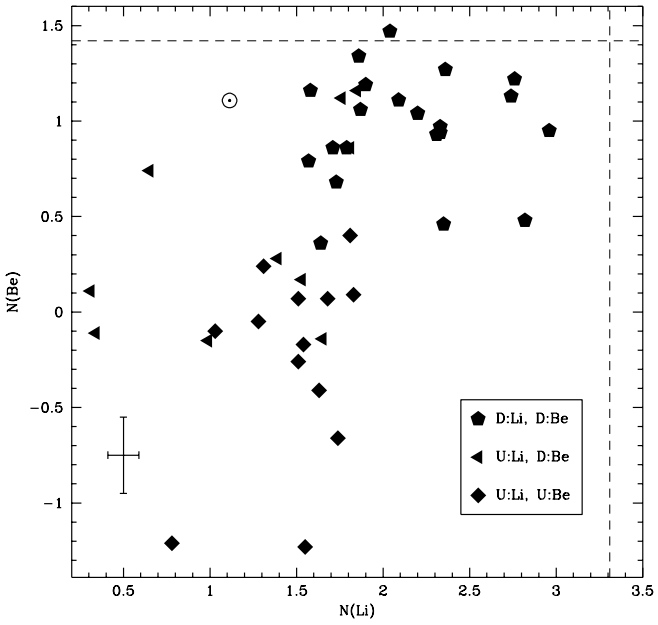

FIG. 8.—Beryllium abundances for the solar metallicity sample are plotted as a function of photospheric lithium. Dashed lines represent the assumed, initial lithium [N(Li) $\sim$ 3.31] and beryllium (N(Be) $\sim$ 1.42) abundance for these Population I stars. Solid pentagons represent simultaneous Li and Be detections, solid, left-facing triangles denote Be detections and Li upper limits, and solid diamonds symbolize concurrent Li and Be upper limits. The error bar reflects the average 1 σ error in a given abundance.

5.1. *Light Element Depletion Models*

F and G dwarfs possess certain structural similarities. The observable surface layers are in contact with a chemically homogeneous and rapidly mixed convective envelope. Between this surface convection zone (SCZ) and the depths of nuclear destruction lies a stable radiative layer that acts as a light element reservoir. Communication between the SCZ and the interior layers, via bulk material flows, may result in surface abundance changes. Standard stellar evolutionary models of low-mass main-sequence stars, however, have a SCZ completely decoupled from the depths of nuclear destruction (Bodenheimer 1965; Chaboyer, Demarque, & Pinsonneault 1995; D'Antona & Mazzitelli 1984; Deliyannis, Demarque, & Kawaler 1990; Forestini 1994; Pinsonneault et al. 1990; Proffitt & Michaud 1991; Swenson et al. 1994). These models do not predict significant light elements deficiencies apart from some pre–main-sequence Li burning. The models of Pinsonneault et al. (1990), shown in Figure 9, illustrate this point. However, the base of the SCZ in G stars occupies a large fraction of the Li preservation region; thus, these cool dwarfs may suffer Li depletion associated with convective mixing and possible overshoot. In contrast, the Be preservation region is much larger than the depth of the convective envelope in G stars, so Be burning at the base of the SCZ is not predicted. Although some Li burning associated with convective mixing may occur in the coolest of our program stars, explaining the observed Li and Be underabundances in F dwarfs certainly requires incorporating additional physics onto the canonical model. While measurements of Li alone may be used to discriminate between scenarios (Balachandran 1995; Deliyannis, King, & Boesgaard 1996), more powerful constraints become available when more than one light element is considered simultaneously. Beryllium, because it is slightly more resilient than Li in stellar interiors, serves as a tracer of the bulk motions occurring at depths beneath the radius of Li destruction. Beryllium observations can, therefore, lift the model degeneracy and assist in isolating the physical mechanism responsible for light element deficiencies (Deliyannis 1995).

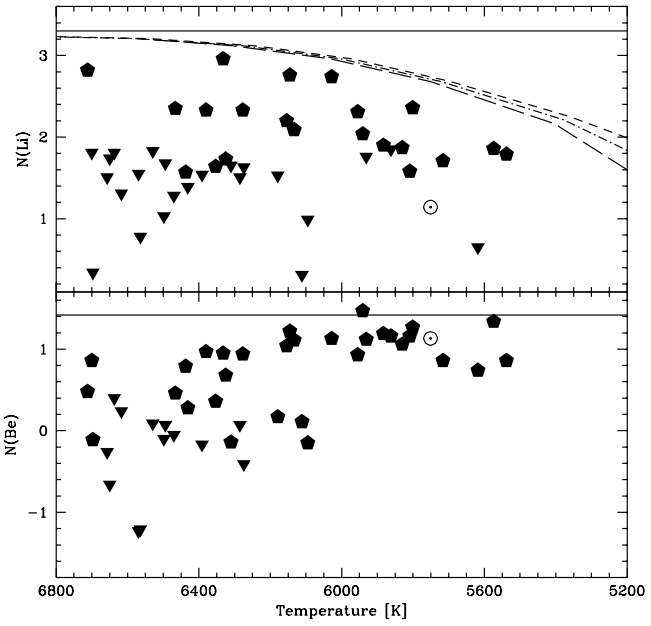

FIG. 9.—Superimposed on the N(Li) and N(Be)-$T_{\rm eff}$ planes are several light element depletion isochrones for nonrotating models as calculated by Pinsonneault et al. (1990). The models shown here represent the amount of photospheric Li and Be that should be present in nonrotating stars evolved from the PMS to 0.07 Gyr (*dashed line*), 0.7 Gyr (*dot-dashed line*), and 1.7 Gyr (*long-dashed line*). Also shown are the observed Li and Be data. Meteoritic abundances are assumed to represent undepleted light element concentrations.

5.1.1. *Mass Loss*

Of the proposed depletion scenarios, mass loss is conceptually the simplest. The SCZ in F star models is much shallower than the Li preservation region, which has a sharp boundary below which no Li is preserved. A wind slowly removes Li (and Be) rich material from the surface of F stars, which erodes the Li preservation region. Once the SCZ penetrates the nuclear destruction zone (NDZ), Li-poor material is mixed into the superficial layers, which dilutes the photospheric Li concentration (Schramm et al. 1990). However, because the relative depth of the NDZ for Li ($\sim$2% by mass) and Be ($\sim$7% by mass) is well separated in F stars (see Fig. 9 of Swenson & Faulkner 1992; hereafter SF92), the Li reserve may be depleted by 5–12 *orders of magnitude* before "significant" (δBe $\sim$ 0.02 dex) Be deficiencies occur (SF92).

As previously mentioned, Figure 7*a* displays the calculated Li and Be abundances in our solar metallicity sample as a function of effective temperature. Restricting our attention to stars that populate a $\sim$600 K wide $T_{\rm eff}$ window centered on 6600 K, the Li gap region, we see that eight members of this subsample have simultaneous Li and Be *detections*. Furthermore, six of these stars have depleted (Li $\leq \frac{1}{6} \times N(\mathrm{Li})_{\rm init}$ and Be $\leq \frac{2}{5} \times N(\mathrm{Be})_{\rm init}$) their initial light element reserves. Although the statistics are not overwhelming, the detection of Li and Be underabundances suggests mass loss is not the primary light element sink in these gap stars. Indeed, as SF92 state, "Any [F] star that has depleted Be via mass loss must necessarily be devoid of Li."

Figure 7*a* also confirms the results of other studies (Deliyannis & Pinsonneault 1993; Garcia Lopez et al. 1995; King et al. 1997), which show that stars cooler than 6000 K may exhibit moderate Be deficiencies. Furthermore Figure 12 (below), a plot of all simultaneous Li and Be detections versus $T_{\rm eff}$, reveals that several stars with slightly depleted Be also have detectable photospheric Li concentrations. If, as SF92 claim, Be should not be depleted in an atmosphere that contains an observable amount of Li, then mass loss would be hard pressed to account for the observed abundance trends. However, using late G stars to constrain mass-loss models is less robust than the aforementioned F stars data since small Be deficiencies are predicted by some mass-losing solar models (Boothroyd, Sackmann, & Fowler 1991).

Of course, the standard arguments against mass loss still apply. The onset of Li depletion should be fairly rapid once the SCZ intersects the radius of Li destruction. Observations of open clusters (see Michaud & Charbonneau 1991, and references therein) suggest that Li depletion is a slow, progressive phenomenon that continues throughout the main-sequence lifetime of F and G stars. Furthermore, to reproduce the intrinsic dispersion seen in galactic cluster stars at a given $T_{\rm eff}$ (e.g., Boesgaard & Tripicco 1986a, Thorburn et al. 1993—Hyades; Balachandran 1995, Deliyannis et al. 1996—M67), one has to arbitrarily fine

tune the mass-loss rates to match observations. SF92 also note that several "unpalatable" conclusions regarding the Hyades initial mass function (IMF) would have to be accepted in order to reconcile mass-losing model predictions with observations of Li in cool Hyades dwarfs. Thus, SF92 suggest mass loss is not a credible explanation of the Hyades G dwarf depletion morphology. Evidence for (1) simultaneously detected, but depleted, Li and Be in F stars, (2) slowly developing Li deficiencies in open clusters, (3) intrinsic abundance dispersions in open clusters, and (4) the IMF absurdities implied by the SF92 models (if forced to explain Li depletion in dwarf G Hyads) all argue against main-sequence mass loss as the cause of Li and Be depletion.

5.1.2. *Microscopic Diffusion*

According to models of microscopic diffusion (e.g., Michaud 1986; Richer & Michaud 1993) several competing forces, which include gravitational settling, thermal diffusion (both of which are directed radially inward), and radiative levitation (outwardly directed), can cause the trace elements Li, Be, and B to sink or buoy—relative to hydrogen—in the radiative regions beneath the surface convection zone. In the absence of turbulence, which can severely retard these diffusive motions, the dominance of one process over the other two may result in a flow of material either into (if either gravitational settling or thermal diffusion dominate) or out of (if radiative acceleration prevails) the surface convection zone. Consequently, light element abundance anomalies may develop. However, the relative efficiency of these various diffusive processes is sensitive to the predominant ionization state of the atom under consideration that, in turn, is a function of the temperature beneath the SCZ (Michaud & Charbonneau 1991). Thus, the depth of the SCZ, which increases dramatically from early F to mid G stars, will significantly affect both the direction and rate of light element diffusion.

Richer & Michaud (1993) predict the diffusive properties of both Li and Be in evolving, nonrotating models that suffer neither internal turbulence nor superficial mass loss. These models are a more sophisticated treatment of the diffusion theory described by Michaud (1986), but the end results are not greatly dissimilar. Above a certain threshold temperature ($\sim$6900 K for Li, $\sim$6700 K for Be), the push of radiative forces on Li and Be at the base of the convective envelope exceeds the local gravity and results in a flow of these elements into the SCZ (Michaud & Charbonneau 1991). Consequently, the radiative buffer zone, the region between the nuclear destruction zone and the base of the surface convection zone, is drained of its light element reserve, while the SCZ light element concentration increases. Therefore, lithium and beryllium abundance concentrations in excess of the cosmic level are predicted for late A and early F stars. In stars with progressively smaller $T_{\rm eff}$, the temperature at the base of the deepening convection zone increases rapidly, thus Li and Be become fully ionized. These bare nuclei, with small geometrical cross sections, are incapable of being supported by radiation pressure. Li and Be, therefore, leak out of the SCZ and are no longer in physical contact the surface layers. Superficial light element underabundances consequently develop. Models of microscopic diffusion predict stars cooler than $\sim$6200 K contain a SCZ so massive (SCZ mass increases with decreasing $T_{\rm eff}$) that the timescale required to significantly deplete the convective envelope is comparable to an evolutionary timescale (Michaud 1986). Thus, the superficial Li and Be concentration in late F and early G stars is expected to remain at or near the cosmic level for as long as these stars remain on the main-sequence. It is this pattern of enhancement ($T_{\rm eff} \geq 6900$ K), settling (6900 K $> T_{\rm eff} >$ 6200 K), and stagnation ($T_{\rm eff} \leq 6200$ K), predicted by diffusion models, that results in the formation of light element abundance gaps.

A simple test of diffusion theory utilizes observations of Li and Be in stars cooler than 6200 K. Models of microscopic diffusion predict little depletion of either Li or Be (Richer & Michaud 1993). Contrary to the model predictions, several of our cool F stars exhibit significant depletion. Lithium deficiencies vary from 1.0–2.0 dex and Be concentrations range from 3–30 times smaller than cosmic levels. The timescale for diffusion of either element is far too long to expect substantial main-sequence depletion (Michaud & Charbonneau 1991), yet it appears as though both Li and Be have been removed from the surface layers of these stars. This argument could be seriously challenged should the timescale for diffusion decrease. Note, however, that the mass of the convection zone dominates the diffusion *e*-folding time (Michaud 1986). Thus, the rates with which both Li and Be settle out of the convective envelope of a cool ($T_{\rm eff} < 6200$ K) star should be similar. Figure 10, which displays the logarithmic ratio of Li-to-Be as a function of $T_{\rm eff}$, reveals that the data are not consistent with equal rates of diffusion. Even when PMS burning is accounted for (*dotted line*), most of our late F and early G stars appear to be more severely Li than Be deficient. If the

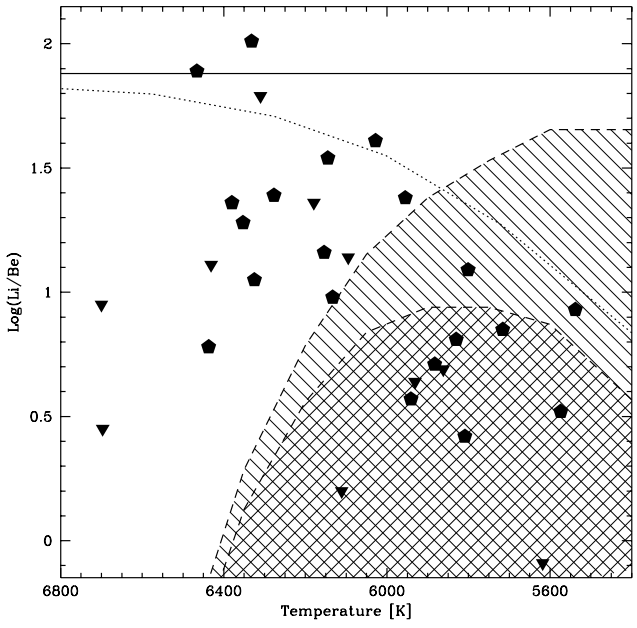

FIG. 10.—Plotted is the logarithm of the Li-to-Be ratio for the solar metallicity sample as a function of effective temperature. Pentagons represent simultaneous Li and Be detections, while inverted triangles denote a Li upper limit and a Be detection. The dotted line represents the Pinsonneault et al. (1990) Li-to-Be ratio for nonrotating stars subjected to pre–main-sequence burning only. The upper dashed line marks the predicted border of the Charbonneau & Michaud (1988) "zone of avoidance" for a mixing length of 1.6. The lower dashed line represents a smaller zone of avoidance created assuming the Pinsonneault et al. (1990) PMS depletion curve represents the initial abundance ratio.

rates of Li and Be depletion were equivalent in cool stars, then log (Li/Be) would not change during the main-sequence lifetime of these stars. Once a star reaches the ZAMS and begins to dilute Li and Be, its position should be fixed in the log (Li/Be)-$T_{\rm eff}$ plane, and should remain near the PMS depletion curve. We interpret the scatter in Figure 10, which cannot be accounted for by observational error alone, as an indication that Li is removed more efficiently than Be from the photosphere of our program stars. Unequal rates of Li and Be settling in these cool stars strongly argues against models of microscopic diffusion.

Recent findings (Balachandran 1995; Deliyannis et al. 1996) suggest that the depletion of Li in old open clusters is a result of Li burning rather than gravitational settling. Models of diffusion (e.g., Richer & Michaud 1993) predict main-sequence F stars will deplete their convective envelope; however, rather than destroy the light element reserve, these stars retain Li and Be in a radiative buffer zone beneath the SCZ. Stars evolving past the main-sequence turn-off should therefore dredge up the Li and Be reservoir, restoring the surface concentrations to near cosmic levels (Deliyannis et al. 1990). Post–turn-off stars in M67 that have yet to enter the phase of subgiant dilution do not exhibit Li abundances characteristic of the assumed initial cluster value (Balachandran 1995). It appears, therefore, that Li deficiencies in post–turn-off stars are the result of Li burning rather than simple, nondestructive diffusion into the radiative buffer zone. Evidence for Li consumption in evolved stars is another, independent strike against the theory of microscopic diffusion as the sole cause of main-sequence Li and Be abundance anomalies.

5.1.3. *Meridional Circulation*

Thermal imbalances, fueled by stellar rotation, distort normally spherical equipotentials common in nonrotating stars, and drive large-scale "meridional circulation" currents in stellar interiors. Originally described by Eddington (1925) and Vogt (1925), the phenomenon of meridional circulation is another potential explanation of the F star Li and Be abundance gaps.

Currents induced by rotation are assumed to penetrate the polar region of a star's SCZ and exit toward the equatorial plane. Light-element underabundances occur when the bulk motions drive Li (or Be) depleted material from regions beneath the radius of nuclear destruction into the surface convection zone. The exiting streamlines also drag Li- and Be-rich material from the surface layers into the radiative interior. The net result of this process is a slow dilution of the superficial light element concentration (Charbonneau & Michaud 1988, hereafter CM88). Models of meridional circulation make explicit, testable predictions regarding the concurrent removal of Li and Be from cool dwarf photospheres and, therefore, can be directly compared to our data.

CM88, however, add another level of complexity to their models by simultaneously considering the effect of both meridional circulation and microscopic diffusion on the light elements. Incorporating the physics of microscopic diffusion leads to a conditionality whereby a star's rotational velocity determines whether meridional circulation or diffusion governs superficial light element concentrations. It is predicted that stars which rotate rapidly enough ($v_{\rm crit} \sim 15$ km s^{-1} at 7000 K and $v_{\rm crit} \sim 5$ km s^{-1} at 6400 K) exhibit abundance patterns dominated by circulation currents; however, if the star rotates slower than the critical velocity, diffusion (which includes the phenomena of gravitational settling, thermal diffusion, and radiative levitation) will dictate the abundance trends. However, diffusion rates in cool dwarfs ($T_{\rm eff} < 6200$ K) are so slow, due to the sheer mass of the convective envelope (Michaud 1986), that meridional circulation currents should govern the abundance patterns.

The CM88 models predict meridional circulation will diminish the surface concentration of the light elements by infusing the convective envelope with Li- and Be-poor material. The onset of Li and Be depletion, though, is staggered because of the differing sizes of the respective preservation zones, the layers above the depths of nuclear burning. The shallow Li reservoir is the first to be diluted; therefore, if meridional circulation is operating in these stars, the Li abundance will begin to decline while the Be concentration will, initially, hover near cosmic levels. Once Be depletion commences, the Li/Be ratio stabilizes since the flux of Li into the radiative interior matches that of Be (CM88). Using the models of CM88, we recreate their Figure 13, which depicts the minimum Li/Be ratio attainable in stars as a function of $T_{\rm eff}$. The dashed curves in our Figure 10 define a "zone of avoidance" which should not be penetrated if meridional circulation is responsible for the observed light element depletion. Superimposed upon the theoretical predictions are our data, presented here as the logarithmic ratio of Li-to-Be versus $T_{\rm eff}$. We exclude stars with simultaneous upper limits, which provide no useful information. Nearly all of the stars with a $T_{\rm eff} < 6200$ K penetrate the zone of avoidance suggesting that some cool stars have depleted more Li than would be expected if meridional circulation were operating alone. Pre–main-sequence burning, while an obvious source of further Li depletion in the coolest of these stars, was not included in the CM88 models. Subtracting the CM88 prediction from the 0.7 Gyr PMS depletion curve of Pinsonneault et al. (1990) results in a smaller zone of avoidance as shown in Figure 10 (*lower dashed curve*). Nevertheless, several of the coolest stars inhabit the smaller forbidden region. The repeated violation of the predicted zone of avoidance by our cool dwarf data suggest that either Li and Be dilution does not occur at comparable rates or Li burning is more efficient than the CM88 models suggest. Regardless, the data call into question the validity of these meridional circulation models.

As demonstrated in the above paragraphs, our late F and early G star data appear to directly contradict the CM88 predictions. Stars hotter than 6900 K provide another useful diagnostic of the composite meridional circulation + diffusion model. In these early F stars radiative acceleration prevails over gravitational settling, which results in predicted Li and Be overabundances. Meridional circulation can temper this outward diffusion as long as the star rotates rapidly enough for circulation currents to efficiently dilute the surface abundances. However, Balachandran (1990) reports stars hotter than the dip, which rotate too slowly to counteract Li enhancements due to radiative levitation, show no significant evidence for overabundances. Moreover, the few early F stars with secure Be measurements and small rotation velocities do not appear to have Be overabundances (Boesgaard 1976; Boesgaard & Budge 1989). Thus, Li and Be observations in stars both warmer and cooler than the dip argue against the

CM88 formalism. While improvements in the input physics may alleviate some of the discrepancies, the models, as they currently stand, are not a viable explanation for observed light element trends.

5.1.4. *Rotationally Induced Turbulent Mixing*

Rotation, a fundamental property of most stars, greatly complicates the calculation of stellar structure and evolution. In the absence of a simpler theory, rotationally induced instabilities have come to be recognized as a complex, yet plausible, explanation for light element abundance anomalies observed in F dwarfs.

Turbulence resulting from shear flow instabilities, a consequence of meridional circulation, was explored by Vauclair (1988) as a possible cause of Li deficiencies in main-sequence F stars. However, the models of Pinsonneault et al. (1989, 1990) and Charbonnel et al. (1992, 1994) have merged a prescription of turbulent mixing with realistic models of evolving stars. As noted in the introduction to Pinsonneault et al. (1990, hereafter PKD), "Real stars rotate." Not only do real stars rotate, but, as was shown by Kraft (1967), surface rotation velocities decrease with time. It is the interaction between the surface layers spun down by a corotating, magnetically driven wind and a rapidly rotating interior, as prescribed by Endal & Sofia (1981), which may drive material mixing in F and G stars (PKD). The stellar wind saps the convective envelope of angular momentum, reducing the angular velocity of the surface layers. An angular velocity gradient between the SCZ and the rapidly rotating interior subsequently develops. If the gradient becomes too steep, a shear instability develops and may redistribute angular momentum from the interior to the surface layers. It is assumed that material mixing is weakly coupled to this angular momentum flux (Pinsonneault et al. 1989, hereafter PKSD). The efficiency with which Li- and Be-poor material, matter from beneath the radius of nuclear destruction, mixes into the stellar photosphere is a function not only of stellar mass but also of the initial angular momentum (PKD).

Observations of cool dwarfs reveal that initial angular momentum increases with increasing stellar mass (PKD, and references therein). In other words F stars have more angular momentum initially than G stars. In a sense, the F stars have more angular momentum to lose, and, since material mixing is coupled with angular momentum loss, F stars should suffer more superficial light element deficiencies than G stars. Thus, a Li dip begins to form in mid-F stars. Of course, this mixing presupposes an angular momentum sink that would, ultimately, drive the flow. A magnetic field embedded within the surface convection zone may act as a lever arm to torque down the surface layers, which results in the development of a subsurface shear. As one moves from late to early F stars, though, convection zone mass and magnetic field strength rapidly declines. This observed trend is thought to be related to the rotational break seen in stars with Li gap effective temperatures ($\sim$6600 K) (Kraft 1967; Boesgaard & Tripicco 1986a). Stars hotter than the gap tend not to suffer a surface velocity decrease with age, so the amount of angular momentum loss (or predicted material mixing) associated with late A and early F stars is significantly reduced. It is the increased initial angular momentum with increasing mass (and its subsequent loss) that causes significant light element depletion in stars with $T_{\rm eff} \leq 6600$ K, while the rotational break retards the efficiency of angular momentum loss for hotter stars. The net result is a Li abundance gap in stars with surface temperatures near 6600 K.

The models of PKSD and PKD consider the effects of rotation and angular momentum loss on photospheric Li and Be abundances. PKD model the amount of Li and Be depletion due angular momentum loss in stars with masses between 0.4 and 1.3 $M_{\odot}$. Improvements in the input physics have been made since the original publication of the PKD (a.k.a. "Yale") models. Chaboyer, Demarque, & Pinsonneault (1995) recalculate the depletion curves for low-mass stars ($0.5 \leq M/M_{\odot} \leq 1.3$) using OPAL opacities, while Deliyannis & Pinsonneault (1993, 1997) concentrate on modeling the cool side of the Li dip. The morphology of light element depletion predicted by the updated models of Deliyannis & Pinsonneault (1993) are superimposed on the abundance versus $T_{\rm eff}$ plots in Figure 11. The models are described in terms of initial equatorial rotation velocities for a given mass instead of initial angular momentum (upper models have $v_{e,\rm init} = 10$ km s^{-1}, lower models $v_{e,\rm init} = 30$ km s^{-1}). The isochrones are depletion predictions for stars with ages of 0.1 Gyr, 1.7 Gyr, 4.0 Gyr and near-solar metallicities; hence, hereafter we compare only the solar [Fe/H] data with the Yale model predictions using the meteoritic values as the initial abundances. The theoretical isochrones reproduce the shape of the observed Li and Be depletion curves rather well and manage to bracket the observed abundance spread, although Be deficiencies in excess of the model predictions are observed in some cool stars ($T_{\rm eff} \leq 6200$ K).

The rotationally induced mixing (RIM) models predict the presence of a Li and Be gap, deficiencies in excess of

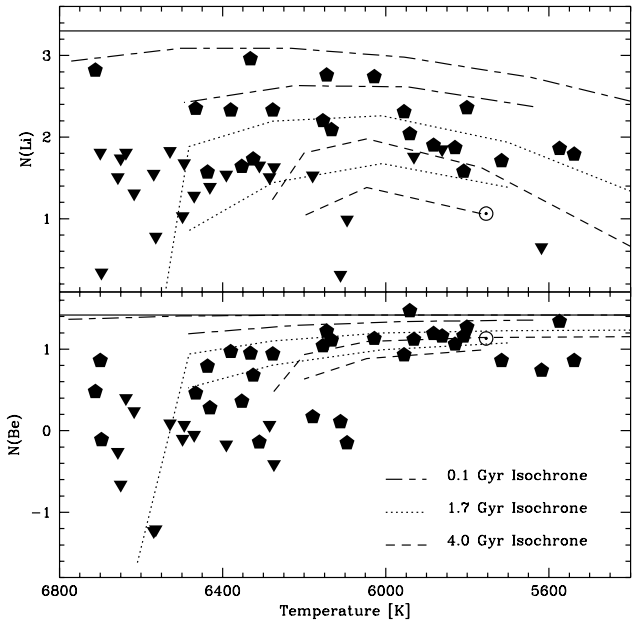

FIG. 11.—Rotationally induced mixing isochrones of Deliyannis & Pinsonneault (1993, 1997) are plotted on the N(Li) and N(Be)-$T_{\rm eff}$ planes. In each case the upper curve for a given age (*long/short-dashed lines*, 0.1 Gyr isochrones; *dotted lines*, 1.7 Gyr isochrones; *dashed lines*, 4.0 Gyr isochrones) represents a model with an initial equatorial velocity of 10 km s^{-1}, while the lower curves are predictions for a model with an initial equatorial velocity of 30 km s^{-1}. Also plotted are the Li and Be data for the solar metallicity sample.

2 dex, near 6600 K that is fully developed by 1.7 Gyr (Deliyannis & Pinsonneault 1993). The Yale models also suggest stars with $T_{\rm eff} < 6100$ K should retain more than one half of its original Be. While a gap is likely present in both our Li and Be data, consistent with the RIM models, the cool star Be data reveal Be deficiencies in excess of the Yale model predictions. It is possible that systematic errors lurking in the geochemical analysis of carbonaceous chondrites could affect the assumed initial abundances. Unfortunately, our sample, stars that are known to deplete their superficial Li abundance, can not constrain the cosmic Be abundance and few, Li-rich stars have been observed for Be. Although there is some uncertainty in the cosmic Be abundance of solar metallicity stars (see § 5), we can conclude that the Yale models do reproduce the light element depletion trends if not the absolute Li and Be deficiencies.

Ambiguity in the cosmic level also complicates the analysis of another Yale model prediction: Stars that have a significantly depleted, but observable, amount of Li and Be should not be uncommon. These so-called 110 Herculis stars are named after the first star observed to exhibit a detectable Li abundance but a depleted Be abundance (Boesgaard & Lavery 1986). A focus of this study was to determine whether or not 110 Her was anomalous. We now expect that it is not, and that stars which deplete most, but not all, of their original Li also destroy a small fraction of their initial Be. Figure 12 shows all of the simultaneous detections in our solar metallicity stars with effective temperatures between 6600 and 5400 K. This sample was further subdivided into abundance classes. The open diamonds in Figure 12 denote stars with Be abundances exceeding 1.11 dex, while solid diamonds represent detections ranging between 0.81 and 1.11 dex. Stars with detections smaller than 0.81 dex are shown as filled hexagons. Also included in the figure is one open hexagon which represents the peculiar star HR 646, or HD 13555, that has a securely detected (and depleted) Be abundance but exhibits only a moderate Li deficiency. Eight stars with detected Be abundances, those stars listed in Table 6 as "probable" 110 Her analogs, retain at most 20% of their original Li and less than 50% of their initial Be allotment assuming the meteoritic abundance reflects the initial Be concentration. While probable 110 Her analogs exist at all temperatures, "bona fide" 110 Her analogs, stars depleted by more than a factor of 2 relative to the mean photospheric Be abundance reported by Boesgaard (1976) (N(Be) $\approx$ 1.11), occupy a small $T_{\rm eff}$ window centered on 6400 K. Thus, even when we consider the initial Be abundance to be a factor of 2 smaller than the meteoritic level, a few F stars still exhibit detected, depleted Li and Be abundances, which suggests 110 Her is not alone. Despite worries about the cosmic Li and Be level, Figure 12 also shows that the possible 110 Her analogs

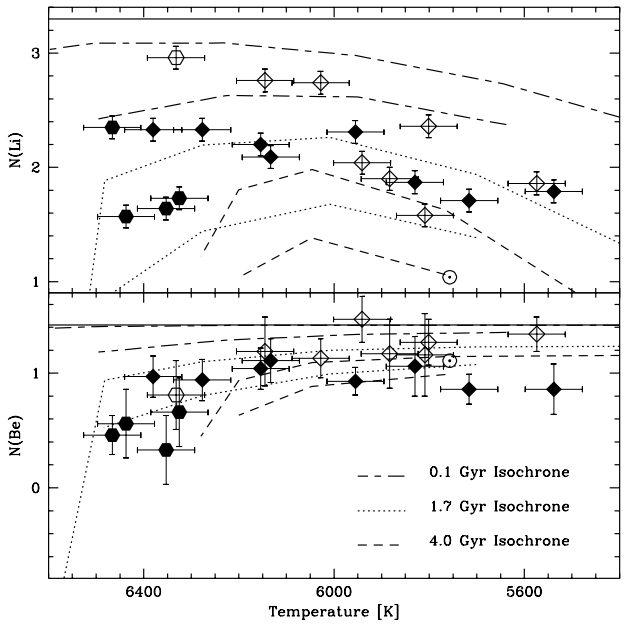

FIG. 12.—Stars with simultaneous Li and Be *detections* are shown versus $T_{\rm eff}$ as are the Deliyannis & Pinsonneault (1993, 1997) model predictions. This subsample was divided into three classes: stars with N(Be) $\geq$ 1.11 (*open diamonds*), stars with N(Be) $\in$ (0.81, 1.11) (*solid diamonds*), and stars with N(Be) $\leq$ 0.81 (*solid hexagons*). These subsets represent (in order of decreasing Be abundance) (i) stars with undepleted Be (with respect to the meteoritic Be abundance), (ii) stars with mild ($\geq$0.3 dex) Be depletions (again with respect to the meteoritic level) (a.k.a. "probable 110 Her analogs"), and (iii) stars with significant Be deficiencies (with respect to both the meteoritic value and the mean Be abundance of F and G dwarfs observed by Boesgaard 1976) (a.k.a. "bona fide 110 Her analogs). Error bars represent the mean $T_{\rm eff}$ uncertainty ($\pm$60 K) and the calculated uncertainty in the Li and Be abundance estimates for each star. Also shown (open hexagon) is the peculiar star (HR 646 = HD 13555) that has a depleted Be concentration and only moderate Li deficiencies.

TABLE 6

POSSIBLE 110 HERCULIS ANALOGS

HD Number	HR Number	[Fe/H]	log (g)	$T_{\rm eff}$	N(Li)	N(Be)	σN(Be)	Type[a]
19994	962	+0.15	4.12	6133	+2.09	+1.11	0.19	P
30649	...	−0.46	4.27	5716	+1.71	+0.86	0.13	P
110897	4845	−0.46	4.27	5830	+1.87	+1.06	0.26	P
117176	5072	−0.04	4.02	5538	+1.79	+0.86	0.22	P
165908	6775	−0.47	4.38	5955	+2.31	+0.93	0.12	P
173667	7061[b,c]	−0.08	4.04	6353	+1.64	+0.33	0.30	BF
182101	7354[c]	−0.19	4.25	6325	+1.73	+0.66	0.30	BF
198390	7973	−0.22	4.35	6380	+2.33	+0.97	0.18	P
204121	8205	+0.06	4.18	6466	+2.35	+0.46	0.17	BF
211976	8514	−0.39	4.07	6277	+2.33	+0.94	0.18	P
220117	8885[c]	−0.02	4.15	6437	+1.57	+0.56	0.30	BF
222368	8969	−0.13	4.19	6154	+2.20	+1.04	0.18	P

[a] Type of 110 Herculis analog: (P) "probable" 110 Her analog [N(Be) $\in$ (0.81, 1.11)]; (BF) "bona fide" 110 Her analog (N(Be) $\leq$ 0.81).

[b] 110 Herculis.

[c] Spectrum synthesis abundance and error estimate.

predominantly fall along similar isochrones in both the N(Li) and N(Be) versus $T_{\rm eff}$ plots. Although there is not a direct, one-to-one correlation, most of the 110 Her candidates appear to lie along the space spanned by the 1.7 and 4.0 Gyr isochrones. The existence of 110 Her analogs and their general agreement with the position of the Yale model isochrones in the N(Li) and N(Be) versus $T_{\rm eff}$ diagrams, suggest that a slow, rotationally induced mixing may operate during the main-sequence lifetime of F and G stars.

Tidally locked binary stars with short orbital periods ($\approx$8–9 days) provide a key piece of evidence corroborating the assertion that rotationally induced mixing occurs in main-sequence F and G stars. The short-period tidally locked binaries (SPTLBs) synchronized early during the PMS contraction phase (Zahn & Bouchet 1989). With the rotational angular momentum of each member transferred to the orbital angular momentum shared by both, neither star should experience significant material mixing associated with superficial, main-sequence angular momentum loss (Deliyannis 1990; Deliyannis, Demarque, & Kawaler 1990). These objects should then retain a majority of their initial Li *if* light element abundance deficiencies are a result of some slow, rotationally induced mixing. Observations of SPTLBs in moderately old galactic clusters reveal that these binaries consistently retain more Li than single cluster members with similar surface temperatures (Deliyannis et al. 1994; Ryan & Deliyannis 1995; Barrado y Navascues & Stauffer 1996). The physical process that depletes Li in individual stars appears to have been rendered less efficient in SPTLBs. The depletion of Li in cluster stars must therefore be linked to some slow mixing phenomenon if both the F star and SPTLB data are to be believed. Although it has been noted that older RIM models (PKD) have some difficulty explaining Li abundances in low-mass main-sequence stars in young open clusters (Garcia Lopez, Rebolo, & Martin 1994), models with updated opacities and physics (Chaboyer et al. 1995) are capable of reproducing the Li depletion trends seen in late spectral type stars. Note, too, that an intrinsic abundance spread at a given effective temperature in cluster stars is neatly explained by the Yale models. Single stars with identical mass but with different initial angular momenta will experience different degrees of internal mixing and, consequently, depletion. The Yale models can, therefore, account for (1) the Li and Be depletion patterns seen in Population I F dwarfs, (2) the enhanced Li abundances associated with SPTLBs, and (3) the spread in Li abundances at a given mass observed in clusters. These lines of evidence point toward rotationally induced mixing as a plausible explanation of light element deficiencies in cool, main-sequence dwarfs.

5.1.5. *Internal Gravity Waves*

Descending convective cells in F and G stars repeatedly impinge upon the interface dividing the SCZ and the radiative interior. Waves generated by these pressure fluctuations are thought to result in small-scale shear turbulence and, consequently, material mixing within the otherwise stably stratified interior regions of cool dwarfs (Press 1981; Garcia Lopéz & Spruit 1991; Montalbán 1994; Montalbán & Schatzman 1996). Models of mixing due to internal gravity waves predict the formation of a Li abundance gap similar to those observed in open clusters. However, despite enhancements in the wave flux, this formalism is incapable of producing significant Be underabundances during the main-sequence lifetime of a late F star (Garcia Lopéz & Spruit 1991). Improvements in the theory (Montalbán 1994; Montalbán & Schatzman 1996) reveal that significant shortfalls are still evident. The new model cannot account for a dispersion in Li (or Be) at a given effective temperature. As previously mentioned, galactic cluster observations (e.g., Boesgaard & Tripicco 1986a, Thorburn et al. 1993—Hyades; Balachandran 1995, Deliyannis et al. 1996—M67) demonstrate that Li depletion is not a unique function of mass ($T_{\rm eff}$). Furthermore, the revamped theory predicts stars cooler than 6300 K will exhibit *at most* a Be deficiency of 0.1 dex. If meteoritic abundances reflect the true cosmic value, then our data, as well as the observations of Garcia Lopéz et al. (1995), suggest that Be deficiencies are common in Li-poor stars. In light of these shortfalls, these particular turbulent mixing models are not considered a likely source of light element deficiencies.

6. SUMMARY AND CONCLUSIONS

Moderate and high resolution observations of the Be (3131 Å) region in $\sim$60 field dwarfs reveal several interesting depletion patterns. While a crisp correlation between N(Be) and $T_{\rm eff}$ does not exist in our diverse sample of Li-poor stars, evidence for a Be abundance dip similar to the Boesgaard Li gap is present. In contrast, some stars cooler than 6000 K exhibit moderate (a factor of 2–4) Be deficiencies. These Be depletion patterns, when used in conjunction with Li abundances calculated using literature Li EQWs and updated stellar parameters, constitute a useful discriminant of the published models, which claim to explain light element abundance trends. It should be noted that the proposed depletion mechanisms are not necessarily mutually exclusive. One process working in concert with one or more of the others may reproduce the abundance trends, and it would *not* be surprising if more than one process were operating, at least to some extent, in our program stars. Until such hybrid models exists, we can only hope to use the present data to constrain or argue against the current models. In particular, using predominantly the solar metallicity F star data as a test of several depletion scenarios, we find the following:

Internal gravity waves.—The specific models put forth are incapable of explaining several observations. The existence of Be-poor cool dwarfs cannot be reconciled with the gravity wave hypothesis, which predicts only minor ($<$0.1 dex) depletion in stars of late spectral type. Also an intrinsic Li abundance dispersion, such as that seen in open cluster stars, would, most likely, require arbitrarily fine tuning the theory to match observations.

Mass loss.—While mass loss could explain Li depletion patterns alone, it is hard pressed to account for the observation of Be deficient F stars that also retain a detectable amount of Li. Several other aspects of mass losing models are unpalatable including: (i) Necessary (and ad hoc) fine tuning of mass-loss rates to explain the observed dispersion of Li in open cluster stars of similar effective temperature, and (ii) the peculiar requirements of the Hyades IMF in order that mass-losing models of G dwarfs match observations.

Microscopic diffusion.—Diffusion theory predicts that Li and Be should settle out of the surface convection zone at equal rates. Observations of cool F stars ($T_{\rm eff} \leq 6200$ K) reveal that Li is depleted more rapidly, or at least commences before, Be dilution. It is, therefore, unlikely that

diffusion is the predominant source of Li and Be depletion in that subsample. The lack of significant Li and Be overabundances in hot ($T_{\rm eff} > 6900$ K) stars, which would be caused by radiative levitation, further constrains models of diffusion. Also, observations of post–turn-off stars in galactic clusters reveal that Li is *destroyed* during a star's stay on the main-sequence rather than safely stored in the radiative buffer zone, contrary to the predictions of diffusion models. While it is certainly plausible that diffusion may operate in stable, radiative regions, there may be some other force, such as mild turbulence, which renders diffusive transport ineffective immediately beneath the SCZ of F and G dwarfs.

Meridional circulation.—Models of global circulation currents predict the dilution of Li prior to the commencement of Be depletion. However, once Be depletion begins, the Li-to-Be ratio should remain fixed and should not fall beneath a calculated zone of avoidance. The Li-to-Be ratio in our late F and early G dwarfs repeatedly violate this hypothesized forbidden region. These models also have difficulty explaining the normal Li and Be abundances seen in slowly rotating early F stars.

Rotationally induced turbulent mixing.—To date, this theory is the most plausible explanation for the observed light element trends. The Yale models can account for the Li and Be depletion patterns, the presence of enhanced concentrations of Li in SPTLBs, and the intrinsic Li abundance scatter observed in cluster stars of identical mass. This slow mixing, resulting from superficial angular momentum loss, also predicts the existence of stars that retain an observable amount of Li but have also depleted a fraction of their original Be. We report the discovery of eight "probable" and four "bona fide" 110 Her analogs that add to the evidence in favor of the RIM models.

Although the F star light element data can constrain several of the depletion hypotheses, further work would assist in narrowing down the possible choices. In particular, observations of Be in several clusters would remove the chemical and age ambiguities that clouded this analysis. A systematic search for Be in galactic clusters of increasing age, similar to what has been done for Li, could significantly constrain the existing depletion scenarios. Apart from a large-scale survey for Be in open clusters, other elements may shed light on the true source of light element depletion. Boron, like Li and Be, is destroyed by proton reactions deep within the interiors of F and G dwarfs. Being somewhat more stalwart than either Li or Be, boron is a probe of even deeper regions within cool, main-sequence stars. Since boron survives in the outer 17% (by mass), of normal ZAMS stars, spectroscopic observations of this element will probe nearly 9 times as deep as Li and more than twice as deep as Be. *Hubble Space Telescope* observations of B in Li- and Be-deficient F stars (Boesgaard et al. 1998b) will, therefore, serve as a further discriminant of light element depletion scenarios.

We would like to thank the following people and institutions for their support on this project. The National Science Foundation for the grant AST 94-09793, which supports A. M. B. Support for C. P. D. was provided by NASA through grant HF-1042.01-93A awarded by the Space Telescope Science Institute, which is operated by the Association of Universities for Research in Astronomy, Inc., for NASA under contract NAS 5-26555, and by the University of Hawaii Foundation through the Beatrice Watson Parrent Postdoctoral Fellowship.

REFERENCES

Anders, E., & Grevesse, N. 1989, Geochim. Cosmochim. Acta, 53, 197
Andersen, J., Gustafsson, B., & Lambert, D. L. 1984, A&A, 136, 6
Balachandran, S. 1990, ApJ, 354, 310
———. 1995, ApJ, 446, 203
Balachandran, S., Lambert, D. L., & Stauffer, J. R. 1988, ApJ, 333, 267; erratum 470, 1243 (1996)
Barrado y Navascues, D., & Stauffer, J. R. 1996, A&A, 310, 879
Blackwell, D. E., & Lynas-Gray, A. E. 1994, A&A, 282, 899
Blazit, A., Bonneau, D., & Foy, R. 1987, A&AS, 71, 57
Bodenheimer, P. 1965, ApJ 142, 451
Boesgaard, A. M. 1976, ApJ, 210, 466
———. 1996, in ASP Conf. Ser. 92, Formation of Galactic Halo ... Inside and Out, ed. H. Morrison & A. Sarajedini (San Francisco: ASP), 327
Boesgaard, A. M., Beers, T., Deliyannis, C. P., Keane, M., King, J. R., Ryan, S., & Vogt, S. 1998a, in preparation
Boesgaard, A. M., & Budge, K. G. 1989, ApJ, 338, 875
Boesgaard, A. M., Budge, K. G., & Burck, E. E. 1988, ApJ, 325, 749
Boesgaard, A. M., & Chesley, S. E. 1976, ApJ, 210, 475
Boesgaard, A. M., Deliyannis, C. P., Lambert, D. L., & Stephens, A. 1998b, ApJ, in press
Boesgaard, A. M., Heacox, W. D., & Conti, P. S. 1977, ApJ, 214, 124
Boesgaard, A. M., & King, J. R. 1993, AJ, 106, 2309 (BK93)
Boesgaard, A. M., & Lavery, R. S. 1986, ApJ, 309, 762
Boesgaard, A. M., & Tripicco, M. J. 1986a, ApJ, 302, L49
———. 1986b, ApJ, 303, 724
Bonifacio, P., & Molaro, P. 1997, MNRAS, 285, 847
Bonneau, D., Balega, Y., Blazit, A., Foy, R., Vakili, F., & Vidal, J. L. 1986, A&AS, 65, 27
Boothroyd, A. I., Sackmann, I. J., & Fowler, W. A. 1991, ApJ, 377, 318
Carlsson, M., Rutton, R. J., Bruls, J. H. M. J., & Shchukina, N. G. 1994, A&A, 288, 860
Carney, B. W. 1982, AJ, 87, 1527
Cayrel de Strobel, G., Hauck, B., François, P., Thévinin, F., Friel, E., Mermilliod, M., & Borde, S. 1992, A&AS, 95, 273
Charbonnel, C., Vauclair, S., Maeder, A., Meynet, G., & Schaller, G. 1994, A&A, 283, 155
Charbonnel, C., Vauclair, S., & Zahn, J.-P. 1992, A&A, 255, 191
Charbonneau, P., & Michaud, G. 1988, ApJ, 334, 746 (CM88)
Chaboyer, B., Demarque, P., & Pinsonneault, M. H. 1995, ApJ 441, 876
D'Antona, F. D., & Mazzitelli, I. 1984, A&A 138, 431
Deliyannis, C. P. 1990, Ph.D. thesis, Yale Univ.
———. 1995, in ESO/EIPC Workshop, The Light Element Abundances, ed. Philippe Crane (Berlin: Springer), 395
Deliyannis, C. P., Demarque, P., & Kawaler, S. 1990, ApJS, 73, 21
Deliyannis, C. P., King, J. R., & Boesgaard, A. M. 1997, in Wide Field Spectroscopy, ed. M. Kontizas et al. (Dordrecht: Kluwer), 201
Deliyannis, C. P., King, J. R., Boesgaard, A. M., & Ryan, S. G. 1994, ApJ, 434, L71
Deliyannis, C. P., & Pinsonneault, M. H. 1993, in IAU Colloq. 137, Inside the Stars, ed. W. W. Weiss (San Francisco: ASP), 174
———. 1997, ApJ, 488, 833
Duncan, D. K. 1981, ApJ, 248, 651
Eddington, A. S. 1925, Observatory, 48, 73
Edvardsson, B., Andersen, J., Gustafsson, B., Lambert, D. L., Nissen, P. E., & Tomkin, J. 1993, A&A, 275, 101 (EAGLNT)
Endal, A. S., & Sofia, S. 1981, ApJ, 243, 625
Forestini, M. 1994, A&A 285, 473
Garcia López, R. J., Rebolo, R., & Martin, E. L. 1994, A&A, 282, 518
Garcia López, R. J., Rebolo, R., & Pérez de Taoro, M. R. 1995, A&A, 302, 184
Garcia López, R. J., Severino, G., & Gomez, M. T. 1995, A&A, 297, 787
Garcia López, R. J., & Spruit, H. C. 1991, ApJ, 377, 268
Hauck, B., & Mermilliod, M. 1990, A&AS, 86, 107
Hobbs, L. M., & Duncan, D. K. 1987, ApJ, 317, 796
King, J. R. 1993, AJ, 106, 1206
King, J. R., Deliyannis, C. P., & Boesgaard, A. M. 1997, ApJ, 478, 778
Kiselman, D. 1994, A&A, 286, 169
Kiselman, D., & Carlsson, M. 1995, in ESO/EIPC Workshop, The Light Element Abundances, ed. Philippe Crane (Berlin: Springer), 372
Kraft, R. P. 1967, ApJ, 150, 551
Kurucz, R. L. 1993, CD-ROM (Cambridge: Smithsonian Astrophys. Obs.)
Kurucz, R. L., Furenlid, I., Brault, J., & Testerman, L. 1984, Solar Flux Atlas from 296 nm to 1300 nm (Sunspot: National Solar Observatory Atlas)
Lambert, D. L., Heath, J. E., & Edvardsson, B. 1991, MNRAS, 253, 610
Magain, P. 1987, A&A, 181, 323
Mermilliod, J.-C., & Mermilliod, M. 1994, Catalog of Mean *UBV* Data on Stars (New York: Springer)

Michaud, G. 1986, ApJ, 302, 650
Michaud, G., & Charbonneau, P. 1991, Space Sci. Rev., 57, 1
Montalbán, J. 1994, A&A, 281, 421
Montalbán, J., & Schatzman, E. 1996, A&A, 305, 513
Nissen, P. E. 1981, A&A, 97, 145
Pallavicini, R., Cerruti-Sola, M., & Duncan, D. K. 1987, A&A 174, 116
Pinsonneault, M. H., Kawaler, S. D., & Demarque, P. 1990, ApJS, 74, 501 (PKD)
Pinsonneault, M. H., Kawaler, S. D., Sofia, S., & Demarque, P. 1989, ApJ, 338, 424 (PKSD)
Press, W. H. 1981, ApJ, 245, 286
Proffitt, C. R., & Michaud, G. 1991, ApJ, 371, 584
Rebolo, R., Molaro, P., & Beckman, J. E. 1988, A&A, 192, 192
Richer, J., & Michaud, G. 1993, ApJ, 416, 312
Ryan, S. G., & Deliyannis, C. P. 1995, ApJ, 453, 819
Saxner, M., & Hammarbäck, G. 1985, A&A, 151, 372
Schramm, D. N., Steigman, G., & Dearborn, D. S. P. 1990, ApJ, 259, L55
Sneden, C. 1973, ApJ, 184, 839
Soderblom, D. R., Jones, B. F., Balachandran, S., Stauffer, J. R., Duncan, D. K., Fedele, S. B., & Hudon, J. D. 1993, AJ, 106, 1059
Spite, F., & Spite, M. 1982, A&A, 115, 357
Swenson, F. J., & Faulkner, J. 1992, ApJ, 395, 654 (SF92)
Swenson, F. J., Faulkner, J., Rogers, F. J., & Iglesias, C. A. 1994, ApJ, 425, 286
Taylor, B. 1994a, PASP, 106, 452
———. 1994b, PASP, 106, 704
———. 1995, PASP, 107, 734
Thorburn, J. A., Hobbs, L. M., Deliyannis, C. P., & Pinsonneault, M. H. 1993, ApJ, 415, 150
Vauclair, S. 1988, ApJ, 335, 971
Vogt, H. 1925, Astron. Nach., 223, 229
Zahn, J.-P., & Bouchet, L. 1989, A&A, 223, 112